การเตรียมตัวเร่งปฏิกิริยาโคบอลต์สนับสนุนด้วยรูทีเนียม
โดยวิธีการเผาไหม้แบบอัตโนมัติสำหรับการสังเคราะห์ฟิสเชอร์-ทรอปช์

นางสาวรุ่งระวี เพียรลุผล

วิทยานิพนธ์นี้เป็นส่วนหนึ่งของการศึกษาตามหลักสูตรปริญญาวิทยาศาสตรดุษฎีบัณฑิต
สาขาวิชาเคมีเทคนิค ภาควิชาเคมีเทคนิค
คณะวิทยาศาสตร์ จุฬาลงกรณ์มหาวิทยาลัย
ปีการศึกษา 2557

PREPARATION OF RUTHENIUM PROMOTED COBALT CATALYSTS BY AUTOCOMBUSTION METHOD FOR FISCHER-TROPSCH SYNTHESIS

Miss Rungravee Phienluphon

A Dissertation Submitted in Partial Fulfillment of the Requirements
for the Degree of Doctor of Philosophy Program in Chemical Technology
Department of Chemical Technology
Faculty of Science
Chulalongkorn University
Academic Year 2014

Thesis Title	PREPARATION OF RUTHENIUM PROMOTED COBALT CATALYSTS BY AUTOCOMBUSTION METHOD FOR FISCHER-TROPSCH SYNTHESIS
By	Miss Rungravee Phienluphon
Field of Study	Chemical Technology
Thesis Advisor	Professor Tharapong Vitidsant, Ph.D.
Thesis Co-Advisor	Professor Noritatsu Tsubaki, Ph.D.

Accepted by the Faculty of Science, Chulalongkorn University in Partial Fulfillment of the Requirements for the Doctoral Degree

.....Dean of the Faculty of Science
(Professor Supot Hannongbua, Dr.rer.nat.)

THESIS COMMITTEE

.....Chairman
(Associate Professor Kejvalee Pruksathorn, Dr. de L'INPT)

.....Thesis Advisor
(Professor Tharapong Vitidsant, Ph.D.)

.....Thesis Co-Advisor
(Professor Noritatsu Tsubaki, Ph.D.)

.....Examiner
(Assistant Professor Prasert Reubroycharoen, D.Eng.)

.....Examiner
(Assistant Professor Chawalit Ngamcharussrivichai, Ph.D.)

.....External Examiner
(Assistant Professor Montree Thongkam, Ph.D.)

รุ่งระวี เพียรลุผล : การเตรียมตัวเร่งปฏิกิริยาโคบอลต์สนับสนุนด้วยรูทีเนียมโดยวิธีการเผาไหม้แบบอัตโนมัติสำหรับการสังเคราะห์ฟิสเชอร์-ทรอปช์ (PREPARATION OF RUTHENIUM PROMOTED COBALT CATALYSTS BY AUTOCOMBUSTION METHOD FOR FISCHER-TROPSCH SYNTHESIS) อ.ที่ปรึกษาวิทยานิพนธ์หลัก: ศ. ดร. ธราพงษ์ วิทิตศานต์, อ.ที่ปรึกษาวิทยานิพนธ์ร่วม: ศ. ดร. โนริทัทซึ ซึบากิ, 108 หน้า.

งานวิจัยนี้ศึกษาการสังเคราะห์ตัวเร่งปฏิกิริยาฟิสเชอร์-ทรอปช์ โดยวิธีการเผาไหม้แบบอัตโนมัติ ใช้กรดซิตริกเป็นตัวรีดิวซ์ และไนเตรตไอออนเป็นตัวออกซิไดซ์ ตัวเร่งปฏิกิริยาที่เตรียมได้สามารถใช้ในการสังเคราะห์ฟิสเชอร์-ทรอปช์ได้โดยไม่ต้องผ่านกระบวนการรีดักชัน และศึกษาผลกระทบของตัวสนับสนุน ชนิดของตัวรีดิวซ์ และปริมาณกรดซิตริกที่ใช้ ต่อโครงสร้างตัวเร่งปฏิกิริยาและประสิทธิภาพในการสังเคราะห์ฟิสเชอร์-ทรอปช์ พบว่าเมื่อเติมตัวสนับสนุนเพียงเล็กน้อยทำให้การรีดิวซ์ของตัวเร่งปฏิกิริยาในระหว่างกระบวนการเผาไหม้แบบอัตโนมัติสูงขึ้น ส่งผลให้ประสิทธิภาพของตัวเร่งปฏิกิริยามีค่าสูงขึ้นอย่างมีนัยสำคัญ และค่าการเปลี่ยนของคาร์บอนมอนอกไซด์ (CO conversion) เพิ่มขึ้นจาก 0.8 เป็น 41.4 % เมื่อเติมรูทีเนียมเป็นตัวสนับสนุนตัวเร่งปฏิกิริยาโคบอลต์ นอกจากนี้ปริมาณของกรดซิตริกในสารตั้งต้น (อัตราส่วนโดยโมลของกรดซิตริกต่อไนเตรตไอออน: CA/N) ยังมีบทบาทสำคัญในการควบคุมโครงสร้างและประสิทธิภาพการสังเคราะห์ฟิสเชอร์-ทรอปช์ของตัวเร่งปฏิกิริยา ผลการศึกษาตัวเร่งปฏิกิริยาโคบอลต์/รูทีเนียมพบว่า เมื่ออัตราส่วนโดยโมลของกรดซิตริกต่อไนเตรตไอออนเพิ่มขึ้น การรีดิวซ์ของโคบอลต์บนผิวของตัวรองรับเพิ่มขึ้น ผลึกของโคบอลต์มีขนาดเล็กลง แต่ประสิทธิภาพของตัวเร่งปฏิกิริยาเพิ่มขึ้นในช่วงแรกและค่อย ๆ ลดลง ในขณะที่ทั้งการรีดิวซ์และประสิทธิภาพของตัวเร่งปฏิกิริยาเหล็กมีค่าลดลง ปริมาณของตัวรีดิวซ์ที่มากเกินไปจะส่งผลให้มีคาร์บอนหลงเหลือบนพื้นผิวตัวเร่งปฏิกิริยาและลดความสามารถในการทำปฏิกิริยา เมื่อเปรียบเทียบตัวเร่งปฏิกิริยาเหล็กที่เตรียมด้วยวิธีการตกตะกอนร่วมและตัวเร่งปฏิกิริยาที่เตรียมด้วยวิธีการเผาไหม้แบบอัตโนมัติซึ่งไม่ได้ผ่านกระบวนการรีดักชัน พบว่าตัวเร่งปฏิกิริยาที่เตรียมด้วยวิธีการเผาไหม้แบบอัตโนมัติอัตราส่วนโดยโมลของกรดซิตริกต่อไนเตรตไอออนเท่ากับ 0.1 มีประสิทธิภาพสูงกว่าตัวเร่งปฏิกิริยาเหล็กที่เตรียมด้วยวิธีการตกตะกอนร่วม ผลการศึกษาชนิดของตัวรีดิวซ์ (กรดซิตริก กรดออกซาลิก และกรดฟอร์มิก) ที่อัตราส่วนโดยโมลของกรดซิตริกต่อไนเตรตไอออนเท่ากับ 0.3 พบว่ากรดซิตริกเป็นตัวรีดิวซ์ที่ให้ตัวเร่งปฏิกิริยาที่มีประสิทธิภาพสูงสุด ในขณะที่ตัวเร่งปฏิกิริยาที่เตรียมโดยกรดออกซาลิกมีอัตราการเลือกเกิดมีเทนต่ำที่สุด ดังนั้นตัวเร่งปฏิกิริยาสำหรับสังเคราะห์ฟิสเชอร์-ทรอปช์ที่เตรียมโดยวิธีการเผาไหม้แบบอัตโนมัติ สามารถนำมาใช้ในการสังเคราะห์ฟิสเชอร์-ทรอปช์โดยตรงที่มีประสิทธิภาพสูงได้ ทั้งยังเป็นการลดกระบวนการรีดักชันที่มีขั้นตอนซับซ้อนและใช้พลังงานสูง จึงสามารถนำไปพัฒนาได้ต่อไปในอนาคต

ภาควิชา เคมีเทคนิค	ลายมือชื่อนิสิต .....
สาขาวิชา เคมีเทคนิค	ลายมือชื่อ อ.ที่ปรึกษาหลัก .....
ปีการศึกษา 2557	ลายมือชื่อ อ.ที่ปรึกษาร่วม .....

5373822223 : MAJOR CHEMICAL TECHNOLOGY
KEYWORDS: FISCHER-TROPSCH SYNTHESIS / AUTOCOMBUSTION METHOD / CATALYST

RUNGRAVEE PHIENLUPHON: PREPARATION OF RUTHENIUM PROMOTED COBALT CATALYSTS BY AUTOCOMBUSTION METHOD FOR FISCHER-TROPSCH SYNTHESIS. ADVISOR: PROF. THARAPONG VITIDSANT, Ph.D., CO-ADVISOR: PROF. NORITATSU TSUBAKI, Ph.D., 108 pp.

The Fischer–Tropsch synthesis (FTS) catalysts with high reduction levels were synthesized through an autocombustion method using citric acid (CA) as a reductant and nitrate ions (N) as oxidants. The as-synthesized catalysts were used directly in FTS reaction without further reduction. The effects of the promoter, reductant types and citric acid contents on the catalyst structures and FTS performance were systematically studied. Results indicated that the introduction of a small amount of promoter improved the catalyst reducibility during the autocombustion process, and significantly enhanced the FTS activity. The CO conversion of the catalyst increased rapidly from 0.8 to 41.4 % after Ru promotion for Co catalysts. The citric acid contents (molar ratio of citric acid to nitrates: CA/N) in the precursor also played an important role in controlling the structures and FTS performance of the catalysts. For the RuCo catalysts, when the CA/N molar ratio was increased, the metal reduction level increased and the Co crystalline size decreased but the activity of the catalyst first increased and then decreased while metal reduction level and the activity of the iron-based catalysts were decreased. An excessive amount of the reductant could result in more residual carbon species and decrease the activity of the catalyst. Compared with the iron-based catalyst prepared by the conventional co-precipitation method (C_N), the CO conversion of the autocombustion catalyst with CA/N = 0.1 was higher than that of the catalyst C_N. For different types of reductants (at the same molar ratio of reductants to nitrates = 0.3), the catalyst prepared by citric acid exhibited the highest activity whereas the catalyst synthesized by oxalic acid showed the lowest methane selectivity. The FTS catalysts prepared by the autocombustion method, which omits the complex and high-energy consumption reduction process, can be used directly for highly efficient FTS and thus will be more promising in the future.

Department:	Chemical Technology	Student's Signature	.....
Field of Study:	Chemical Technology	Advisor's Signature	.....
Academic Year:	2014	Co-Advisor's Signature	.....

ACKNOWLEDGEMENTS

The author would like to express heartfelt gratitude and sincere appreciation to her advisor, Prof. Dr. Tharapong Vitidvant and co-advisor, Prof. Dr. Noritatsu Tsubaki for their extremely valuable helpful discussion, encouraging guidance, kind supervision and support throughout this study. The author also greatful to Assoc. Prof. Dr. Kejvalee Pruksathorn, Asst. Prof. Dr. Prasert Reubroycharoen, Asst. Prof. Dr. Chawalit Ngamcharussrivichai and Asst. Prof. Dr. Montree thongkham for serving as the dissertation chairman and members of thesis committee, respectively, and for their worthy advice and discussions.

The author appreciatively acknowledge the financial supports from the Thailand Research Fund (through the Royal Golden Jubilee Project), Graduate School, Chulalongkorn University, Department of Applied Chemistry, School of Engineering, University of Toyama, the Higher Education Research Promotion and the National Research University Project of Thailand, the Office of the Higher Education Commission (EN 272 A), the Ratchadaphiseksomphot Endowment Fund (CU-CLUSTER-FUND), the Research Program on Materials for Future Energy and the Center of Excellence on Petrochemical and Materials Technology.

Many thanks also go to the Department of Chemical Technology, Faculty of Science, Chulalongkorn University and Department of Applied Chemistry, School of Engineering, University of Toyama, for providing research facilities throughout this research work.

Most of all, the author would also express her deep sense of gratitude to her family for their love, support and encouragement along graduate study. Special thanks are also extended to her friends who always provide encouragement and support throughout this study.

CONTENTS

Page

Page

Page

Page

LIST OF TABLES

LIST OF FIGURES

LIST OF SYMBOLS AND ABBREVIATIONS

All variables and symbols used in this thesis are listed below. Some symbols have multiple definitions. It should, however, be apparent from the context which of the definition to use.

ASF	:	Anderson-Schulz-Flory equation
BET	:	Brunauer-Emmett-Teller
CA/N	:	Citric acid to nitrate compounds molar ratio
Co	:	Cobalt
Co/SiO_2	:	Cobalt on silica support
Fe	:	Iron
FID	:	Flame ionization detector
FTS	:	Fischer-Tropsch synthesis
Ni	:	Nickel
Q-50	:	Silica support with mean surface area: 78.67 m^2/g
Ru	:	Ruthenium
SEM/EDX	:	Scanning electron microscopy with energy-dispersive X-ray analysis
TCD	:	Thermal conductivity detector
TG/DTA	:	Thermogravimetic and Differential Thermal Analysis
TPR	:	Temperature-programmed reduction

W/F	:	Ratio of weight of catalyst (g) to flow rate of reactant (mol/h)
WGS	:	Water-gas shift reaction
XPS	:	X-ray Photoelectron Spectroscopy
XRD	:	X-ray Diffraction
α	:	Chain growth probability factor

CHAPTER I
INTRODUCTION

Growing demand of energy coupled with the possibility of running out of oil has essentially raised the interest in the production of renewable and clean fuels. Fischer–Tropsch synthesis (FTS) has received more attention than ever since it is considered as an effective process to produce wide-range liquid hydrocarbon fuels and high value-added chemicals from relatively abundant resources, such as natural gas, coal and biomass, *via* synthetic gas (H_2 + CO). The Fischer-Tropsch Synthesis (FTS) is basically the hydrogenation of carbon monoxide, producing mainly hydrocarbons, alcohols, and other oxygenated species. There are many active metals having a sufficiently high hydrogenation activity to be employed in FTS processes such as ruthenium (Ru), iron (Fe), cobalt (Co), nickel (Ni). However, Ni promotes the reaction of carbon monoxide to produce large quantities of methane, and the high price of Ru limits industrial application. This leaves only Co and Fe catalysts consequently employed as FTS catalysts at the industrial scale. Cobalt-based catalysts have high activities and selectivities to large molecular weight hydrocarbons. When the coal gasification is the source of syngas containing a low ratio of H_2/CO, the iron-based catalyst with high water-gas shift reaction (WGS) activity is preferable due to the less hydrogen need.

The high activity of cobalt catalysts requires both appropriate sizes of cobalt crystallites and high dispersion of cobalt active sites [1]. The high dispersion of cobalt

needs a large surface area of the support and a strong interaction between cobalt and the support but a strong metal-support interaction may decrease the reducibility and activity of the catalyst. Although cobalt precursors are easily reduced by the weak interaction supports, it results in very small precursor crystallites which are not stabilized during impregnation and drying steps. Thus, the optimum cobalt dispersion is favored by the combination of support-precursor with intermediate interaction strength. Noble metals promotion (such as ruthenium), which can enhance both the reduction and dispersion of cobalt, is an effective method to enhance the activity of the cobalt catalysts [2]. Additionally, synergistic bimetallic interactions between cobalt and ruthenium can also increase the FTS activity and C_{5+} selectivity. The conventional preparation of cobalt-based FTS catalysts involves impregnation, drying, calcination and reduction steps. Among these steps, the catalyst reduction is especially important, but it increases the cost and complexity of FTS. Therefore, a promoted Co based catalyst with a high metal reduction level without reduction processes will be more promising for FTS.

Iron catalysts are active for FTS and water–gas shift (WGS). It is inexpensive catalytic metal relative to the other catalysts. The activation step is required to obtain the active form of the iron catalyst. Metallic iron is not stable in the presence of CO at typical FT reaction temperatures and readily transforms to iron carbide (FeC) under activation or FTS conditions [3]; consequently, iron carbide is potentially the most important iron phase as far as the bulk FTS is concerned. To attain an

acceptable activity and stability, the iron catalysts need alkali promotion (e.g., 1–5 wt% potassium) and copper (Cu) addition for reduction promotion [4]. For potassium (K) promoter, with the suitable content can maintain the catalyst activity over long periods of time. Furthermore, it not only strengthens the Fe-C bond in iron carbide, but it also weakens the C-O and Fe-H bonds. Weakening C-O increases the rate of reaction since breaking the C-O bond is a rate-limiting step for FTS with Fe. Strengthening the Fe-C bond facilitates chain growth of products while weakening the Fe-H bond reduces H_2 adsorption on the catalyst surface, result in less methane and paraffin formation. Other alkali metals act similarly to K, but less effectively [5]. Copper significantly lowers reduction temperature especially the reduction of Fe_2O_3 to Fe_3O_4, reduces sintering, and permits high surface area without affecting selectivity of the catalysts. Subsequently, K and Cu promoted Fe based catalysts are also the suitable catalysts for the FTS.

Autocombustion is a novel method to produce catalysts with high reduction levels [6, 7]. In the autocombustion synthesis, a low temperature is required to initiate the combustion (exothermic decomposition of a redox mixture of metal salts and reductants), and then the combustion can continue without external energy supply. Therefore, this method has the advantages of low cost and high energy efficiency [8]. Furthermore, during the combustion process, the metal can be reduced by the released gases (such as H_2, CH_4, CO, and so on) from the pyrolysis of the reductant. Therefore, the as-synthesized catalyst might be used directly for the

FTS reaction without further reduction. However, the autocombustion process is very complex and usually occurs violently. It is more difficult to control the reduction level than the conventional H_2 reduction.

Numerous studies have been conducted to improve the metal reduction level during the autocombustion, which include varying the type of organic reductants [8, 9], the reductant contents [6, 10-13], and the pH value of the precursors [14-16]. Nevertheless these methods cannot change the reduction temperature and the rate of cobalt essentially. A promoted autocombustion method by introducing a second metal Ru, which can decrease the reduction temperature of Co and increase the reduction rate by H_2 spillover, may obviously improve the reduction of Co and enhance the FTS activity. In addition, if combined with the optimization of types of organic reductants and the reductant contents, it might be prepared FTS catalysts with high reduction levels and activities.

This thesis focuses on developing a better understanding of the catalyst preparation with high reduction levels by an autocombustion method. The first part of this study focused on investigation of the Ru promoted Co/SiO_2 catalyst with various reductant contents and different reductant types. The Ru promoted Co/SiO_2 catalyst can be identified as ruthenium promoted silica supported cobalt catalyst. The second part of this study was to synthesize the iron-based catalyst (Fe-Cu-K) with the different citric acid content that used as a reductant. The study was scoped as follows:

1. Preparation of the Ru promoted Co/SiO_2 FTS catalysts (10 wt% Co and 1 wt% Ru) with a high reduction level by the autocombustion method.
2. Catalyst characterization of the Ru promoted Co/SiO_2 catalysts using thermogravimetic/differential thermal analysis (TG/DTA), X-ray diffraction (XRD), nitrogen adsorption–desorption, X-ray photoelectron spectroscopy (XPS), scanning electron microscopy equipped with energy-dispersive X-ray analysis (SEM-EDX) and temperature-programmed reduction of hydrogen (H_2-TPR).
3. Preparation of iron-based catalysts (Fe-Cu-K) by the sol-gel autocombustion method.
4. Characterization of the iron-based catalysts using X-ray diffraction (XRD)
5. The effects of the ruthenium promoter, citric acid contents and reductant types on the structures and FTS performance of the catalysts under the reaction conditions of 1.0 MPa, 240 °C, H_2/CO = 2, W/F (CO + H_2 + 3% Ar) = 10 g•h/mol
6. The effects of the citric acid content on the structure and FTS performance of the iron-based catalysts under the reaction conditions of 1.0 MPa, 300 °C, H_2/CO = 1, W/F (CO + H_2 + 3% Ar) = 10 g•h/mol

CHAPTER II
THEORY

This chapter focuses on the fundamental theory of the Fischer-Tropsch Synthesis (FTS) which is well known as one type of carbon monoxide (CO) hydrogenation. The chapter consists of the basic details of synthesis gas, Fischer-Tropsch Synthesis (FTS) as well as the development of FTS catalyst and reactor technologies.

2.1 Synthesis Gas

Synthesis gas or syngas, a mixture comprising of hydrogen and carbon monoxide, can be manufactured from the gasification of widespread natural gas, coal, petroleum, biomass, municipal waste and variety of different materials that contain carbon [17]. Syngas has been widely used since the last century because of the availability and flexibility of the sources. Syngas is well suited as the feedstock for a range of different products, including electricity, transport fuel as well as major developmental clean alternative energy technologies.

Syngas is usually a product of coal gasification and the most important reactions for the gasification of coal as shown in equation (2.1)-(2.4).

$$C + O_2 \longrightarrow CO_2 \quad (2.1)$$

$$2C + O_2 \longrightarrow 2CO \quad (2.2)$$

$$C + H_2O \leftrightarrow CO + H_2 \quad (2.3)$$

$$CO + H_2O \leftrightarrow CO_2 + H_2 \quad (2.4)$$

Furthermore, synthesis gas can also be obtained from reforming of natural gas with either steam or carbon dioxide, or by partial oxidation. The source of syngas produced from natural gas mainly contains by methane as shown in equation (2.5-(2.8). Various sources and processes for syngas production yield different ratios of H_2 to CO [18, 19].

Steam reforming $CH_4 + H_2O \leftrightarrow CO + 3H_2$ (2.5)

CO_2 reforming $CH_4 + CO_2 \leftrightarrow 2CO + 2H_2$ (2.6)

Partial oxidation $CH_4 + 2O_2 \longrightarrow CO + 2H_2$ (2.7)

Water gas shift reaction $CO + H_2O \leftrightarrow CO_2 + H_2$ (2.8)

Usually, a combination of synthesis gas production processes is used to achieve synthesis gas with a stoichiometric ratio of hydrogen and carbon monoxide. A number of publications point the way to possible future commercial applications and to new uses of syngas. The beginning of syngas chemistry occurred in the early 20th century. The hydrogenation of carbon monoxide to produce methane was occurred in 1902, followed by the discovery of ammonia (NH_3) synthesis in 1910. After decade, the Fischer-Tropsch synthesis was developed and then came the manufacture of methanol and higher alcohols. Currently, the uses of syngas are spread in many ways as shown in Figure 2.1.

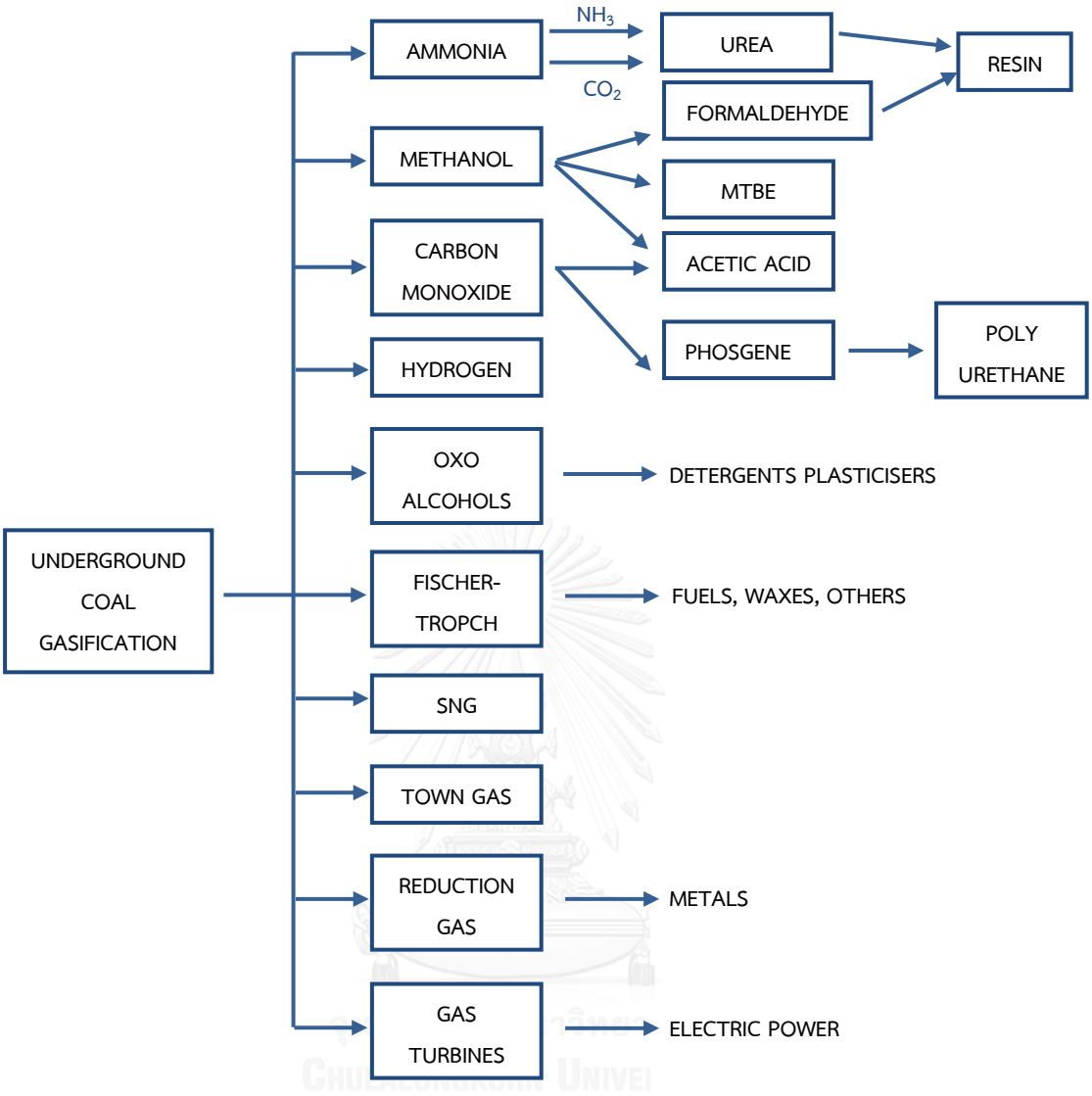

Figure 2.1 Application from synthesis gas

2.2 Fischer-Tropsch Synthesis

Fischer-Tropsch synthesis (FTS) was discovered by Franz Fischer and Hans Tropsch in 1923 at the Kaiser Wilhelm Institute for coal research in Mullheim, Germany. It is basically the hydrogenation of carbon monoxide, producing mainly hydrocarbons (paraffins and olefins), alcohols, and small numbers of other oxygenated species [20]. This process provides transportation fuel and also straight-

chain high molecular weight alcohols and olefins for the chemical industry by converting coal or natural gas *via* syngas. Fischer-Tropsch fuels are considered to have superior quality with no sulfur contamination. Although the cost of the production of fuels from FTS is typically higher than from oil refineries, continuing research of this process has brought the production cost down significantly with developments in reactors, operating conditions, as well as catalysts. The recent FTS researches have focused on the development of both reactors and catalysts to achieve high yields of heavy weight hydrocarbons that can undergo hydrocracking and selective distillation to obtain high quality gasoline and diesel fuels [21].

FTS is a highly exothermic polymerization reaction using CH_x monomer insertion to create the chain growth of products [22], in which methane formation is thermodynamically favored. However, the distribution of hydrocarbon products from FTS can be varied significantly using different catalysts, promoters, H_2/CO ratios, reaction conditions, and types of reactor.

In an attempt to explain the mechanism of this multi-step reaction, many assumptions of the reaction intermediates on catalyst surface for FT reaction were proposed in the past. The Fischer-Tropsch Synthesis (FTS) is regarded as a surface catalyzed polymerization process. The hydrogenation of adsorbed CO produces CH_x monomers, which react with the surface H atoms and hydrocarbon fragments to produce higher hydrocarbons as illustrated in equation (2.9) [23]. The FTS has an

interesting potential in the synthesis of high molecular weight products which can be cracked to yield high-grade diesel fuel in addition to gasoline.

$$CO+2H_2 \leftrightarrow -CH_2- +H_2O \qquad \Delta H= -39.4 \text{ kcal/mol} \qquad (2.9)$$

By the way, a lot of possible reactions occur during FTS reaction. The major reactions of the Fischer-Tropsch synthesis are summarized below.

Paraffins formation:

$$(2n+1)\ H_2+nCO \longrightarrow C_nH_{2n+2}+nH_2O \qquad (2.10)$$

Olefins formation:

$$2nH_2+nCO \longrightarrow C_nH_{2n}+nH_2O \qquad (2.11)$$

Alcohols formation:

$$2nH_2+nCO \longrightarrow CnH_{2n+1}OH+(n-1)H_2O \qquad (2.12)$$

Water gas shift reaction:

$$CO+H_2O \leftrightarrow CO_2+H_2 \qquad (2.13)$$

Boudouard reaction:

$$2CO \leftrightarrow C+CO_2 \qquad (2.14)$$

Coke deposition:

$$H_2+CO \leftrightarrow C+H_2O \qquad (2.15)$$

From the equation above, some oxygenates (equation 2.12) may be also formed during the Fischer–Tropsch process. The hydrocarbon synthesis is catalyzed by metals such as cobalt, iron and ruthenium. Presently, both of iron and cobalt are

used commercially at a temperature of 200 to 300 ℃ and at 10 to 60 bar pressure. For alkalized iron, which is a good water gas shift (WGS) catalyst, the water formed in equations (2.10), (2.11) and (2.12) reacts with CO to form H_2, so the apparent H_2/CO usage becomes smaller. The WGS reaction (equation 2.13) can be used to adjust the ratio of carbon monoxide and hydrogen and its activity can be high over potassium promoted iron catalysts and is negligible over cobalt or ruthenium catalysts. A cobalt catalyst is not a good WGS catalyst. It gives water as a main reaction by-product. From the observation of carbon- and carbide-forming tendency on iron catalysts, Franz Fischer [24] introduced the surface carbidic carbon as reaction intermediates. This carbide form was thought to be hydrogenated to CH_2, which was then further polymerized to various hydrocarbons. For cobalt and ruthenium catalysts, no carbide phases are detected. If synthesis gas with a H_2/CO ratio below 2 is used, the composition is not stoichiometric for the Fischer-Tropsch reactions. Then the water gas shift reaction is important to change the H_2/CO ratio to 2. Figure 2.2 shows the application ranges for iron (high WGS-activity) and cobalt catalysts (no WGS activity). Inexpensive iron catalysts in comparison to cobalt can directly convert low H_2/CO ratio synthesis gas without an external shift reaction.

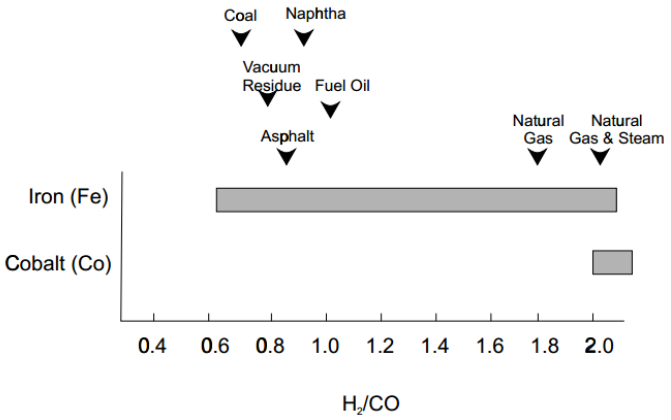

Figure 2.2 Feedstocks and catalysts

2.2.1 Products of Fischer- Tropsch Synthesis

The subsequent FT chain-growth process to heavy hydrocarbons proceeds is comparable with a conventional polymerization process, resulting in a distribution of chain lengths of the products. Generally, the reaction yields compose of hydrocarbons and oxygenated compounds. The major constituents of hydrocarbons are n-paraffins and olefins while the main oxygenated products are alcohols. The distribution of the products depends on the catalyst and the process operation conditions such as temperature, pressure and residence time. The resulting FTS hydrocarbon products generally follow an arithmetical distribution identified as the Anderson-Schulz-Flory (ASF) distribution. The product weight fraction (Mn/n) can be described as:

$$\frac{\mathrm{Mn}}{\mathrm{n}} = (1-\alpha)2\alpha(\mathrm{n}-1)$$

α is the chain growth probability factor ($\alpha = \frac{r_p}{r_p + r_t}$), while r_p and r_t are rate constants of propagation and termination, respectively.

As can be seen in Figure 2.3, according to the Anderson–Schulz–Flory distribution law, more than 50 wt% of the product mixture is C_5–C_{22} hydrocarbons for an α-parameter of 0.7 to 0.875. At higher values of α-parameter the fraction of C_5–C_{22} hydrocarbon products decreases sharply. Low molecular weight and gaseous products, such as methane, are of lower commercial value than longer chain products. Methane is normally underestimated by the ASF distribution and it was slightly decreased at the high alpha values. Therefore, to maximize the productiveness of the FTS, conditions which favour high α-parameters should be used to optimize the selectivity to the more valuable C_5–C_{22} hydrocarbon products [25].

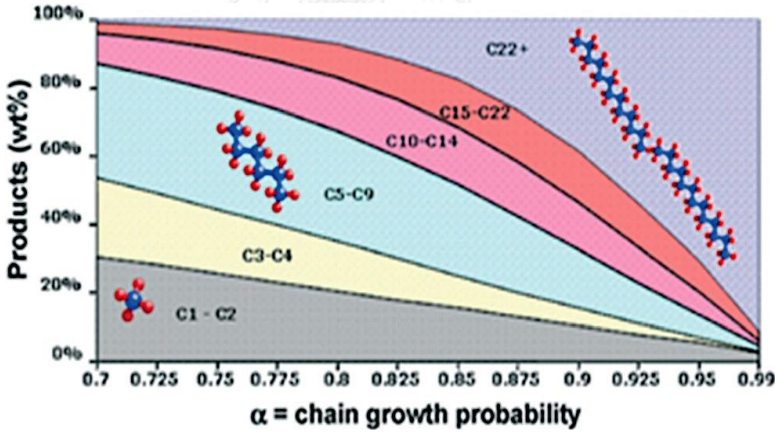

Figure 2.3 Anderson–Schulz–Flory (ASF) values sensitivity

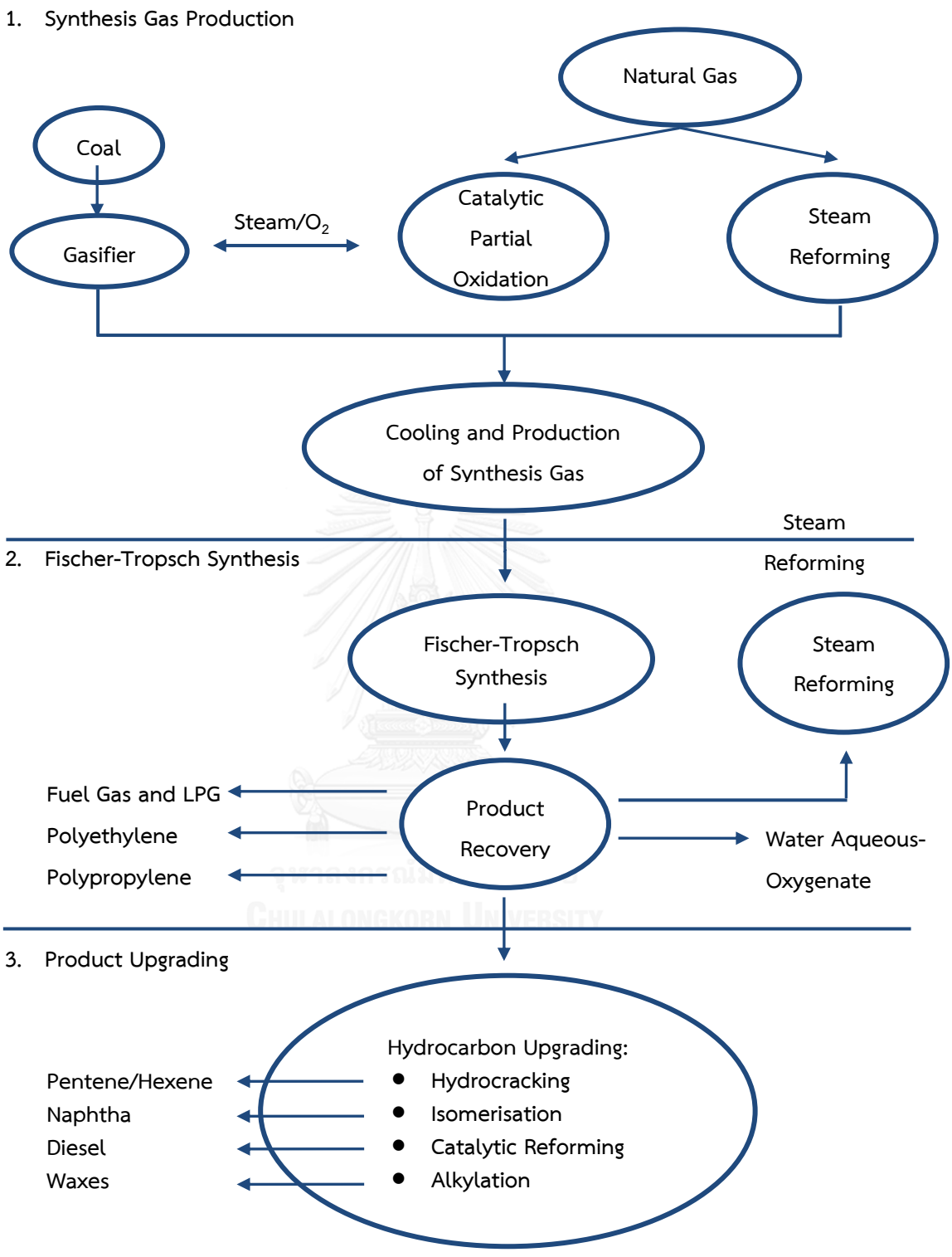

Figure 2.4 Block diagram of the overall Fischer-Tropsch process configuration

The FTS has been developed to allow the transformation of various feedstocks into liquid products, including gas-to-liquid (GTL), coal-to-liquid (CTL) and biomass-to-liquid (BTL) technologies. Natural gas, coal and biomass can be converted to syngas by partial oxidation, steam reforming or gasification processes. Moreover, different hydrocarbons may be directly produced from syngas by developing highly selective FTS catalysts. Therefore, FTS is noted as a valuable process to produce clean fuels from syngas, derived from non-petroleum resources as shown in Figure 2.4. The commercial FT process involves three main sections, namely: synthesis gas production and purification, Fischer-Tropsch synthesis, and product grade-up.

Conventional refinery processes can be used for upgrading of Fischer-Tropsch liquid and wax products. A number of possible processes for FTS products are: hydrocracking, isomerization, catalytic reforming and alkylation. Besides, fuels produced with the FTS are of a high quality due to a very low aromaticity and no sulfur content. The product streams consist of various fuel types: LPG, gasoline, diesel fuel, jet fuel, etc. The diesel fraction has a high cetane number resulting in excellent combustion properties and reduced emissions. New and stringent regulations may promote replacement or blending of conventional fuels by sulfur and aromatic free FTS products. Also, other products besides fuels can be manufactured by FTS in combination with upgrading processes, for example, ethene,

propene, α-olefins, alcohols, ketones, solvents, specialty waxes, and so on. These valuable by-products of the FTS have superior added values, resulting in an economically more attractive process.

2.2.2 Reaction Mechanism

The FT reaction is a polymerization process, involving reactant adsorption, chain initiation, chain growth, chain termination, product adsorption and re-adsorption [26]. Fischer and Tropsch proposed the first supposition, reported in Figure 2.5 [24]. They assumed the dissociative adsorption of the carbon monoxide on the metal atom, with formation of a carbide species. The insertion of the adsorbed dissociated hydrogen into this carbide species produces the active -CH_2- intermediate, which leads to the propagation step. The growing alkyl chain desorbs from the metal by hydrogenation, forming paraffins or olefins. After this first supposition, several different mechanicistic pathways have been elaborated, but all of them contemplate an initiation, propagation and termination step [27].

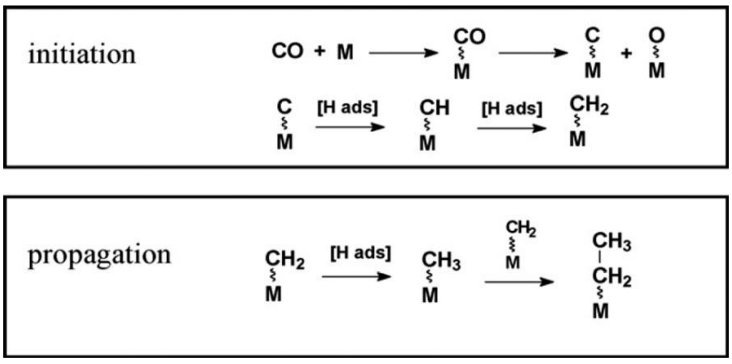

Figure 2.5 Classic mechanicistic pathway of CO hydrogenation

Several reaction pathways have been proposed to explain the observed product distribution in the Fischer-Tropsch synthesis, including the surface carbide mechanism, the surface enol mechanism and the CO insertion mechanism [28].

2.2.2.1 Surface Carbide Mechanism

The surface carbide mechanism is the first, oldest and perhaps most accepted mechanism for iron-based FTS catalysts [29]. The current view for this mechanism is illustrated in Figure 2.6. Initially, the reactions start with dissociative adsorption of CO and H_2. The chemisorbed carbon is subsequently hydrogenated to form chemisorbed CH_2 which oligomerizes to produce higher hydrocarbons. In this mechanism, the CH_2 species can be considered, fixed to either the catalyst surface or the CH_2 (and CH and CH_3) species, are more mobile and are able to move over the catalyst surface [30].

2.2.2.2 Surface Enol Mechanism

In case of enol mechanism, the chain growth starts and takes place through undissociative chemisorption of CO, the surface hydrogen atoms then react with the chemisorbed CO groups to form enolic (HCOH) species as shown in Figure 2.7. The product structure then grows by a combination of surface polymerization condensation and water elimination steps using adjacent groups. There is an alternative route for this mechanism by which the individual hydrogenation of the enolic groups, forming water and CH_2 groups that can grow chains, as was described in the carbide mechanism [31].

2.2.2.3 CO Insertion Mechanism

Based on this mechanism, chain growth takes place through insertion of CO molecules in the metal-carbon bonds. As an initiation step, a CO molecule is inserted into the metal-H bond, and then hydrogenated to produce an alcohol or alkene. As illustrated in Figure 2.8, the initiation step involves the insertion of a CO molecule into a metal-H bond, the resulting aldehyde is then hydrogenated to CH_3 in a rate-determining step. Consequently, CO can be inserted into the metal-carbon bond forming enol species. The enol species can be hydrogenated again. Chain growth happens by repeating this step. Hydrogenation of the growing chain that can result in a free olefin chain and an adsorbed hydrogen atom terminates the chain growth.

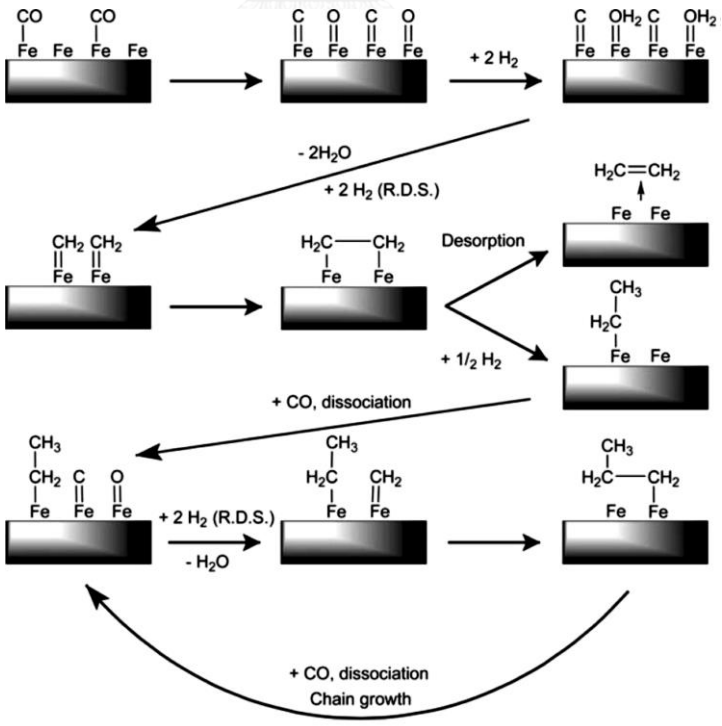

Figure 2.6 The surface carbide mechanism (the rate determining steps (RDS) are indicated in the scheme)

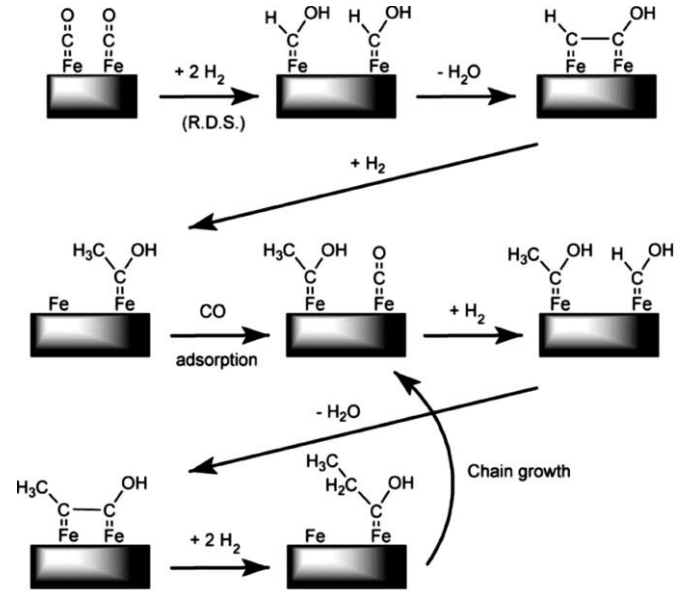

Figure 2.7 The surface enol mechanism (the rate determining steps (RDS) are indicated in the scheme)

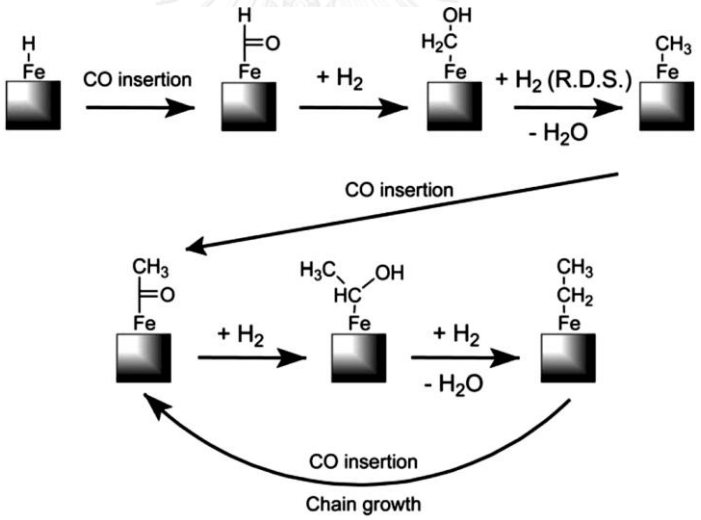

Figure 2.8 The CO insertion mechanism (the rate determining steps (RDS) are indicated in the scheme)

2.3 Fischer-Tropsch Catalyst

The optimum performances of heterogeneous catalysts for a given process require a consideration of a combination of chemical, physical and mechanical properties. Anderson et al. has defined a “triangular concept” for catalyst design, which has been adapted for FTS by Farrauto and Bartholomew [32], as illustrated in

Figure 2.9. In addition the physic-chemical properties of the active phase, specifically formulation shape, size and crystallinity of the nanoparticles are significant factors for optimization during catalyst design.

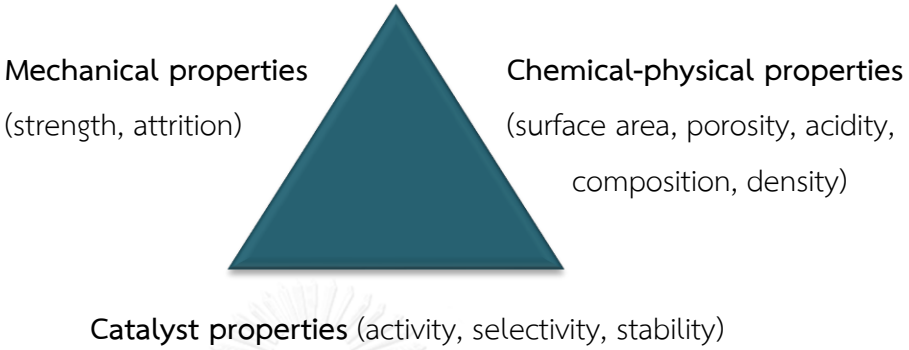

Figure 2.9 Concept of triangle of catalyst design

There are four FTS catalysts which have the activity required for commercial operation that are cobalt (Co), nickel (Ni), iron (Fe), and ruthenium (Ru). Ni was discarded as a FTS catalyst because it has high hydrogenation activity and thus produces predominantly undesired methane. Ru is one of the most active catalysts for FTS operating and has gained more interest in laboratory study at low temperature due to its high activity at low reaction temperature producing long chain hydrocarbons without the need for any promoters. It is characteristically suitable for fundamental study of FTS. However, it is too expensive and its worldwide reserve is insufficient for large-scale industrial use. Therefore it is not considered a sustainable option for use in industrial-scale operations. For these reasons Fe and Co are considered to be the best metals for application in industrial-scale FTS processes. Fe is economically attractive and highly abundant in comparison to other active metals.

Unfortunately, it has a very low selectivity to paraffins, favouring the production of olefins and oxygen, and deactivates more quickly than Co-based catalyst. Although Co is more expensive than Fe, Co has a high FT activity, good selectivity to long hydrocarbon paraffins, low selectivity to olefins and oxygen, and is more resistant to deactivation. Therefore, Co is the preferred choice to produce long chain paraffins, while Fe is the better selection to produce olefins. With Fe and Co catalysts, products vary depending on the promoters, operating temperature and pressure, H_2/CO ratios, and type of reactor. Table 2.1 summarizes distinctive differences properties between Co and Fe catalysts.

Table 2.1 Comparison of the characteristic features of iron and cobalt FTS catalysts

FTS catalysts	**Cobalt**	**Iron**
Cost	More expensive	Less expensive
Activity	Higher conversion rate	Lower conversion rate
Active phase	Cobalt metal	Iron carbides, oxides and oxycarbides
Source of carbon	Natural gas; higher H_2/CO ratios	Coal; lower H_2/CO ratios
Catalyst lifetime	Resistant to deactivation	Less resistant to deactivation
Promoters	Ru, Rh, Pt	Alkalis (i.e., K)
Contents	Cobalt content: <20 wt%	Iron content: >85 wt%
Hydrogenation activity	• Higher hydrogenation activity • Produce more CH_4 at high temperature • Produce more linear paraffins and low oxygenates	• Lower hydrogenation activity • Produces less CH_4 • Produce more olefins and oxygenated species
Water Gas Shift (WGS) activity ($CO+H_2O \leftrightarrow CO_2+H_2$)	Poor WGS catalyst Can operate at high H_2/CO ratios	Good WGS activity Can operate at low H_2/CO ratios

2.3.1 Fe FTS Catalyst

Iron (Fe) is a transition metal with an atomic number of 26. Iron-based catalysts provide low selectivity to undesirable methane and high water gas shift (WGS) activity, producing hydrogen, so the apparent H_2/CO usage becomes lower. It is thus useful for syngas conversion with low H_2/CO ratio 0.5–2.5 syngas obtained from biomass, coal or heavy oil gasification through partial oxidation. However, it is not suitable for conversion of H_2-rich syngas derived from methane.

Although the early development of iron-based catalysts for FTS did not achieve much successful results comparing to their competitors, cobalt catalysts, they have a significant advantage over cobalt catalysts in that Fe is easily available from many sources whereas the supply of cobalt is limited [31]. Fe has a lower cost than Co but has more catalyst attrition problems. Fe catalysts are usually prepared either by precipitation or fusion. The latter preparation was found to produce more attrition resistance catalysts [33]. Typically, precipitated Fe catalysts are prepared by precipitation of mixing solutions containing iron and other promoters. Then it was washed, precipitated, and dried. For fused Fe catalysts, Fe together with promoters is melted in an arc furnace and cooled down in ingots. After cooling down, they are crushed to desired particle sizes. Fused Fe catalysts are the most suitable catalysts for the high temperature Fischer-Tropsch process in circulating fluidized bed or fixed fluidized bed reactors, since other metals would produce high methane [34].

Common activations for iron-based catalysts include CO, H_2, or syngas ($CO+H_2$). Either CO alone or $CO+H_2$ result in iron carbide formation on Fe catalyst surface [35-37]. Furthermore, any metallic iron formed by H_2 reduction of iron oxide catalysts is converted quickly to iron carbide once exposed to syngas [38]. Gradually, iron carbides are converted to a mixture of iron carbides and Fe_3O_4 during synthesis. The extent and rate of formation of the iron oxide phase depend upon the operating conditions such as CO conversion, water gas shift activity, promoter levels and time-on-stream [39]. Therefore, iron in a steady-state is present as a mixture of oxide and carbide phases.

2.3.2 Co FTS Catalyst

Cobalt (Co) is a transition metal element with atomic number of 27. It is similar to silver in appearance. Cobalt forms numerous compounds and complexes of industrial importance. Cobalt exists in the +2 or +3 valance states for the major of its compounds and complexes. A multitude of complexes of the cobalt (III) ion exists, however, few stable simple salt are known. Octahedral stereochemistries are the most common for cobalt (II) ion as well as for cobalt (III). Generally, octahedral cobalt (II) salts and complexes are pink to brownish red, while most of the tetrahedral cobalt (II) species are blue [40].

Table 2.2 Physical properties of cobalt

Parameter	Properties
Name	Cobalt
Symbol	Co
Electron configuration	$[Ar]3d^7 4s^2$
Atomic number	27
First ionization, eV	7.86
Melting point, ℃	1493
Boiling point, ℃	3100
Transformation temperature, ℃	417
Heat of transformation, J/g	251
Latent heat of fusion, ΔH_{fus}, J/g	395
Latent heat of vaporization at bp, ΔH_{vap}, kJ/g	6276
Specific heat, J/(g•℃) at 15-100 ℃	0.442
Coefficient of thermal expansion, ℃	-1
Thermal conductivity at 25 ℃, W/(m.K)	69.16
Thermal neutron absorption, Boht atom	34.8
Resistivity, at 20 ℃, 10^{-8} Ω.m	6.24

Although cobalt is considerably more expensive than iron it is more resistant to deactivation and tends to last longer (iron catalyst only lasts for 8 weeks in

commercial operation) [41]. Co catalysts have received more attention compared to Fe catalysts because of their environmentally friendly by-products as water. Furthermore, advantages of Co catalysts over Fe catalysts are that they have high FTS activity, high selectivity to linear long chain hydrocarbons, and low water gas-shift activity. Thus, Co-based catalysts are preferable choices for the conversion of high H_2/CO ratio syngas as produced from natural gas. As the reasons above, recently many researchers are focus on cobalt metal as FTS catalysts. For the high price of Co, it is desirable to minimize the amount of used Co by use high surface supports such as silica or alumina as well as maximize the surface area of the catalysts [42-44].

Many formulations of cobalt-based catalysts have been studied to improve their performance. The high activity of cobalt catalysts requires both appropriate sizes of cobalt crystallines and high dispersion of cobalt active sites. The high dispersion of cobalt needs a large surface area of the support and a strong interaction between cobalt and the support. This interaction leads to obstruct the low-temperature reduction of the precursor to cobalt metal. High reduction temperatures are required for strong degree of interaction of the support and Co particle. Although cobalt precursors are easily reduced by the weak interaction supports, it results in very small precursor crystallites which are not stabilized during impregnation and drying steps. Thus, the optimum cobalt dispersion is favored by the combination of support-precursor with intermediate interaction strength. Addition of a second metal such as Ru [45], Rh [46] and Pt [47] as a promoter is

reported to improve both the reduction and dispersion of cobalt by increasing hydrogen adsorption on the second metal. It is an effective method to enhance the activity of the cobalt catalysts and C_{5+} selectivity. Furthermore, the impact of preparation variables such as temperature and pH value on catalyst performance has also been investigated [48-50].

2.3.3 Ru FTS Catalyst

Ruthenium (Ru) is high scientific interest as a FTS catalyst, most active and working at the lowest reaction temperature. It produces the highest molecular weight hydrocarbons at reaction temperatures as low as 150 °C. The catalyst is active in its metallic form and no promoters are required to stabilize its activity. Another advantage of Ru is that its lower sensitivity to poisons such as H_2O and CO than iron. However, the use of Ru-based catalysts for FTS is limited to academic studies, since Its high price and limited world resources exclude industrial application [20].

2.4 Development of FTS Catalyst

2.4.1 Catalyst Support

With an absence of diffusion limitation, the rate of a catalyzed reaction should be proportional to the surface area of the active phase. To maximize the active phase for a given mass of active metal, it is necessary to make the particles as small as possible, i.e., to maximize the atoms on the surface: this fraction is termed the dispersion or the fraction exposed. Such fine metal particles can be easily made

using support. The advantages of using the metal supported catalysts include the following [51].

a) The catalyst is easily and safely handled.

b) The catalyst is easily to be recovered by filtration.

c) Metal supported catalysts do not grow in size by sintering when heated to high temperature in high temperature treatments.

d) The support provides chances of bringing promoters into close contact with the active metal.

There have been a number of studies comparing cobalt supported. The most popular commercial supports for FTS consist of SiO_2, Al_2O_3, TiO_2, MgO, active carbon and zeolites [52-56]. The result from Reuel and Bartholomew [53] indicated that the specific activity of cobalt significantly decreases with increasing its dispersion. Product selectivity is the best correlated with dispersion and extent of reduction; the molecular weight of hydrocarbon products is lower and the CO_2/H_2O ratio is higher for the catalysts having higher dispersion and lower extent of reduction. This effect may be due to stable oxides in the well dispersed, poorly reduced catalysts, which catalyze WGS reaction thereby increasing the H_2/CO ratio at the surface. Their results show that significant fractions of CO_2 are produced on highly-dispersed, poorly reduced cobalt catalysts, showing behavior of a typical iron catalyst. The high selectivity to CO_2 of iron catalysts is probably due to the presence of iron oxides which catalyze the WGS reaction. Similarly, the high CO_2 selectivity of

poorly reduced cobalt catalysts may be due to the abundance of stable surface oxides, e.g., cobalt spinels such as cobalt aluminate, which are inactive in CO hydrogenation but it is active in WGS reaction. WGS reaction increases the H_2/CO ratio at the catalyst surface by promoting the formation of light hydrocarbon products such as methane.

Rathousky et al. [54] studied the use of complex metal oxides as support. They found that the catalytic properties of 10 wt% Co/SiO_2-Al_2O_3 was more similar to Co/SiO_2 than to Co/Al_2O_3. The SiO_2-Al_2O_3 multiplex could lead to the formation of more acid sites resulting in the increase of isomerization product.

Lipidus et al. [55] investigated the influence of calcination temperature on the reaction properties of 10%Co/Al_2O_3 and Co/SiO_2. With the increasing of the calcination temperature, the total hydrocarbon yield decreased on Co/SiO_2 catalysts but increased on Co/ Al_2O_3 catalysts. The nature of the oxide phases is thought to be responsible for the variation in catalytic properties. On the surface of the Co/SiO_2 catalyst, Co_3O_4 supposedly reduces the total hydrocarbon yield. The cobalt-support surface compounds cause an increase in the total hydrocarbon yield and the C_{5+} fraction selectivity on Co/Al_2O_3 catalysts. The interaction between the metal and the support for supported Co catalysts has a distinct influence on the reducibility and dispersion of the catalysts and their properties. For example, Bechara et al. [56] found that the cobalt reducibility was influenced by cobalt loading and the porosity of the supports because of the heterogeneity of the cobalt distribution. An increase

in the size of the reduction improves the activity and selectivity for high molecular hydrocarbon weight.

2.4.1.1 Silicon dioxide (SiO_2)

Silicon dioxide or silica is an oxide of silicon with the chemical formula SiO_2. It has been used in many fields since antiquity. Silica is most commonly found as sand or quartz in the nature. The classification of silica was changes the recrystallization formed with descending temperatures. Besides the changes at these critical temperatures, there are probably similar changes from unstable forms towards quartz at atmospheric temperatures, especially after long time intervals. With fairly rapid cooling or heating intermediate forms may not occur in their stable zone, but a direct change from one to another without the intermediate product may take place.

Table 2.3 Physical properties of silicon dioxide

Parameter	Properties
Other names	Silica
Molecular formula	SiO_2
Molar mass	60.1 g/mol
Appearance	White or colorless solid (when pure)
Status	Solid at atmosphere
Density and phase	2.6 g/cm^3
Melting point	1610 °C
Boiling point	2230 °C
Solubility	Insoluble in water
	Insoluble in acid chloride

Silica-supported cobalt catalysts in general exhibit high catalytic activities and liquid/wax hydrocarbon selectivities for FTS [35]. Silica is an ideal support for Co FTS catalysts because of its physical and chemical properties, including its high surface area which favors appropriately high Co dispersion at relatively high loadings of cobalt, and its surface chemistry also helps the reduction of Co^{3+} and Co^{2+} to Co^0.

Choi et al. [57] investigated the reduction of cobalt catalysts supported on Al_2O_3, SiO_2 and TiO_2 and the effect of metal loading on the reduction. The result showed that the activation energy of reduction increased in the following order:

Co/SiO_2 > Co/Al_2O_3 > Co/TiO_2. For different metal loading, the catalyst with the higher loading is more readily reducible than with the lower metal loading.

2.4.2 Catalyst Promoter

Effective reduction of the active phase plays an important role in optimizing catalytic performance, with the addition of small quantities of promoters during the catalyst formulation found to significantly enhance the activity of Co and Fe. Generally, promoters can be divided into structural promoters and electronic promoters [58]. Promoters improve the activity and selectivity of heterogeneous catalysts by influencing the catalyst's structural properties through varying the active phase structure, or modifying the electronic character of the active phase. The functions of the promoters for catalysts are summarized by Zhang et al. [59] as follows:

a) To structurally modify the metal surfaces induced by the promoter;

b) To interact with metal catalyst because the active sites are blocked/covered due to the migration of the modifiers;

c) To improve the reducibility and dispersion of metal cobalt;

d) To transfer charge between the modifier and the metal;

e) To affect the electrostatic fields of modifier ions;

f) To play important roles in the activation of CO and H_2;

g) To improve the longevity of the catalysts.

The structural promoters increase and stabilize the dispersion of the dispersed active site over the catalyst support, while the electronic ones enhance the catalytic properties of the active phase by modifying the chemisorption properties of the catalyst surface. This effect involves the chemisorption bond strength of reactants and intermediates. Generally, metal oxides (MnO and ZnO), alkali metals (Na, K, Rb, Cs) and certain transition metals (Cu, Pd, Pt, Ru) or carbonates are applied as promoters for the Fe and Co-based FTS catalysts

2.4.2.1 Noble Metal Promoter for Co Catalyst

Supported noble metals are excellent FTS catalysts because the noble metals have H_2 spillover effect, which enhances the activity of FTS. However, because of their high cost and unavailable supplies, the noble metals are preferably used as promoters. Usually, the catalysts are promoted with a small amount of noble metal such as Pt, Ru, Re which is claimed to enhance the reducibility and also keep the cobalt metal surface clean during FT reaction [60-63].

Tsubaki et al. [2] proposed the different functions of Ru, Pd and Pt added into cobalt catalysts. The catalytic activity varied in order of RuCo > PdCo > PtCo > Co. The addition of small amount of Ru can remarkably increase the catalytic activity and the reduction degree, whereas Pt and Pd promoted cobalt dispersion. The characterization data showed that Ru enriched on cobalt surface promoted the reduction of Co catalysts, while Pt and Pd uniformly dispersed in the form of Pt-Co

or Pd-Co alloy enhanced the dispersion and scarcely affected the reducibility of Co catalysts.

Li et al. [64] investigated the influence of Ru and Re on the performance of Co/TiO_2 catalysts and found that catalytic activity and C_{5+} hydrocarbon selectivity of Ru and Re promoted catalysts increased. They proposed that Re could suppress the aggregation of metal cobalt and favor the formation of diesel fractions, whereas Ru increased the numbers of active sites and promoted the selectivity of gasoline and diesel fractions.

2.4.2.2 Promoter for Fe Catalyst

Commercial promoters for Fe catalysts are potassium (K) and copper (Cu). For potassium promoter, with the suitable content can maintain the catalyst activity over long periods of time. Furthermore, it not only strengthens the Fe-C bond, but it also weakens the C-O and Fe-H bonds. Weakening C-O increases the rate of reaction since breaking the C-O bond is a rate-limiting step for FTS with Fe. Strengthening the Fe-C bond facilitates chain growth of products while weakening the Fe-H bond reduces H_2 adsorption on the catalyst surface. It results in low methane and paraffin formation. Other alkalis act similarly to K, but less effectively [33]. Copper significantly lowers reduction temperature especially the reduction of Fe_2O_3 to Fe_3O_4, reduces sintering, and permits high surface area without affecting selectivity of the catalysts.

2.5 FTS Catalyst Preparation

The long-standing background of industry in catalyst preparation is the progress of scientific understanding of the processes involved and the development of the relating fundamental sciences (i.e., chemistry of solids, colloid chemistry). The catalyst preparation methods are very diverse and each catalyst can be produced through different routes. Preparation generally includes several successive steps. Numerous supported metal and oxide catalysts are prepared by the sequence of impregnation, drying, calcination, activation, while zeolite catalysts are prepared by precipitation of gel, crystallization, washing, ion exchange, drying. Three fundamental stages of catalyst preparation are summarized as follows:

a) Preparation of the primary solid (or first precursory solid) associating all the useful components (e.g., impregnation, precipitation and co-precipitation, gel formation, selective removal).

b) Processing of that primary solid to obtain the catalyst precursor, for example by heat treatment.

c) Activation of the precursor to give the active catalysts: reduction to metal (hydrogenation catalysts), formation of sulfides (hydrodesulfurization). deammoniation (acidic zeolites). Activation may occur spontaneously at the beginning of the catalytic reaction (selective oxidation catalysts).

The details of the impregnation method, the precipitation method, the surface autocombustion method and the sol-gel autocombustion method are described below [65].

2.5.1 Impregnation Method

Impregnation is the process that a solid is contacted with a fluid containing the components to be deposited over the surface. This term denotes a method whereby a certain volume of solution containing the precursor of the active element of the catalyst is contacted with the solid support. If the solution of the catalyst precursor is added to the support until the point at which the pores are saturated with solution, the technique is referred to an incipient wetness technique. Incipient wetness impregnation (IW or IWI), also called capillary impregnation or dry impregnation, is a commonly used technique for the synthesis of heterogeneous catalysts. When the interaction strength of the active precursor in solution with the support is weak, the method of incipient wetness impregnation followed by drying can be used to apply high loadings of precursors; the maximum loading is limited by the solubility of the precursor in the pore filling solution. On the other hand, increasing the weight loading requires higher concentrations. However, in the absence of sufficiently strong interactions, the drying step usually results in severe redistribution of the impregnated species, and the support can become non-homogeneous covered by the active material in the final catalyst. The wet impregnation technique, soaking or dipping, is an excessive solution added.

A procedure similar to incipient wetness impregnation, but the volume of the solution is more empirically determined to correspond to that beyond which the catalyst begins to look wet. After impregnation method, the solid is separated from solution, and the excess solvent is removed by drying.

The concentration profile of the impregnated compound depends on the mass transfer conditions inside the pores during impregnation and drying. When strong precursor-support interactions occur through chemical or physical forces (surface hydrolysis, ligand substitution, ion exchange, electrostatic attraction), the amount immobilized on the pore walls of the support can exceed that of the dissolved substance which remains in the pore filling solution; the resulting catalyst is designated as sorption type. Under non-equilibrium conditions of impregnation, the distribution of the impregnated component is dictated by a sorption-diffusion system and is only slightly influenced during drying [66].

2.5.2 Precipitation Method

The simple principle of precipitation is that a solution of the catalyst salt is chemically modified to allow it to precipitate out of solution and onto the support. In almost all cases, the formation of a new solid phase in a liquid medium results from two elementary processes which happen simultaneously or sequentially: (1) nucleation, i.e., formation of the smallest elementary particles of the new phase which are stable under the precipitation conditions; and (2) growth or agglomeration of the particles. The problem of obtaining a homogeneous precipitate with respect

to the size and structure of the particles reduces to that of achieving a uniformly high level of supersaturation throughout the liquid before the nucleation starts, which may be quite difficult because of mass and heat transport limitations.

2.5.3 Autocombustion Method

Autocombustion is a novel method to produce catalysts with high reduction levels [6]. In the autocombustion synthesis, a low temperature is required to start the combustion (exothermic decomposition of a redox mixture of metal salts and reductants), and then the combustion can continue without external energy supply. Therefore, this method has the advantages of low cost and high-energy efficiency [8, 67]. Furthermore, during the combustion process, the metal can be reduced by the released gases (such as H_2, CH_4, CO, and so on) from the pyrolysis of the reductant. The as-prepared catalyst might be used directly for the FTS reaction without further reduction. However, the autocombustion process is very complex and usually occurs violently. It is more difficult to control the reduction level than the conventional reduction.

Many studies have been conducted to improve the metal reduction level during the autocombustion, which include varying the type of organic reductants [8, 9], the reductant contents [12, 68-70], and the pH value of the precursors [14]. The researches about the autocombustion are collected as follows:

Shi et al. [6] prepared the supported catalysts (Co/SiO_2) by a novel surface impregnation combustion method using citric acid (CA) as a reductant. The results

showed that during the combustion process, the metal can be reduced by the released gases (H_2 and CH_4) from the decomposition of the CA. With increase of the content of CA, the catalysts reducibility which was measured by temperature-programmed reduction (TPR) and the dispersion of the cobalt metallic increased gradually. The CO conversion of the autocombustion Co/SiO_2 catalyst (without reduction) was almost 3-fold of that of the conventional impregnation method.

Chandradass et al. [8] studied a sol-gel autocombustion route to synthesize zirconia doped alumina nanopowder, using various fuels such as citric acid, acetylacetone, oxalic acid and urea. The phase analysis and particle size in the presence of different fuel were compared. The results showed 100% tetragonal phase as well as particle size of 60 nm in the presence of citric acid. Fuel type is influential on the phase formation and properties of the resultant powders.

Wu et al. [71] investigated the influence of complexing agents such as citric acid, glycine and hydrazine in aqueous medium that functioned as a fuel using the sol-gel autocombustion method. The complexing agents in the starting solution influenced the magnetic interaction between Ni–Zn ferrite and silica, and also affected the particle size.

Mali et al. [69] used a novel sol-gel combustion process to synthesize the ultrafine particles of barium hexaferrite. The nitrate–citrate gels were prepared from metal nitrate and citric acid solutions under various molar ratios. The results showed that the nitrate citrate gels exhibit a self-propagating behavior after ignition in air at

room temperature. The formation temperature and the crystallite size of barium hexaferrite are influenced significantly by the molar ratio of the metal nitrate to citric acid. The formation temperature of barium hexaferrite decreases with increasing the molar ratio of the metal nitrate to citric acid.

Zhong et al. [72] studied the effect of molar ratios of citric acid to the metal nitrate on $BaFe_{12}O_{19}$ nanocrystalline powders by sol-gel autocombustion method using citric acid as a fuel. The ions distribution of citric acid at different pH explains the effect of citric acid in the starting solution. The XRD patterns show different phases for different citric acid content. The powder with high citric acid content took on good magnetic properties. With the increasing of citric acid content, particle sizes of barium ferrite were decreased and magnetic properties were improved. Furthermore, Bahadur et al. [68] synthesized the single-domain barium ferrite nanoparticles with narrow particle-size distribution using an autocombustion technique. In this process, citric acid was used as a fuel. The catalyst exhibited the maximum magnetic properties at moderate citric acid content.

2.6 FT Reactor Technologies

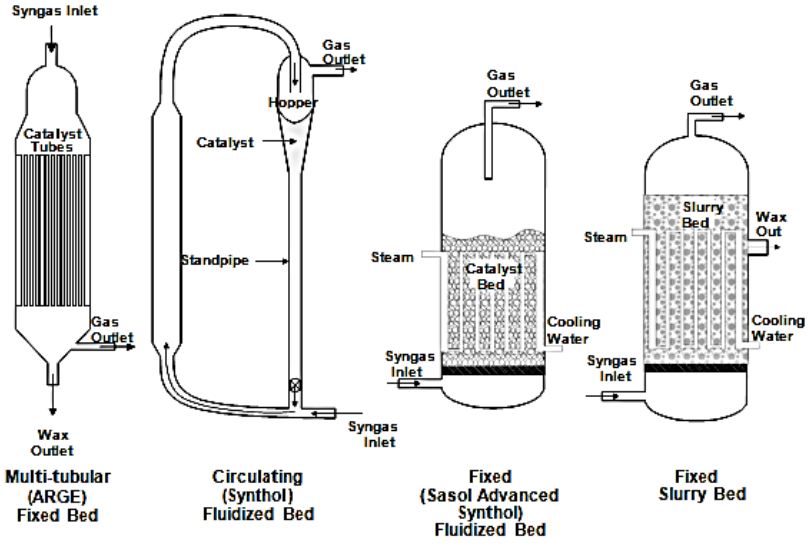

Figure 2.10 The possible reactors for FTS

Reactor type and operation are governing factors in the control of product distribution during FTS. The challenge in FTS reactor design is the efficient and rapid removal of the large heat of reaction (-ΔH = 165-204 kJ/mol) accompanying the process. High temperatures in the reactor lead to excessive methane yields, carbon deposition and catalyst loss due to particle fragmentation. Three main catalytic reactor configurations as shown in Figure 2.10 have been designed and used commercially: fixed bed, fluid bed and slurry bubble columns [73].

2.6.1 Fixed Bed Tubular Reactor

The fixed-bed tubular reactor known as the ARGE reactor is one of the earliest FTS reactor designs and the most competitive reactor technologies in industrial practices. Syngas is introduced into the top of the reactor, flows through the tubes, and the products exit at the bottom of the reactor. Fixed bed reactors

operate at a temperature of about 220-260 ℃ and reactor pressures in the range 25-45 bar. Additional temperature control is obtained by using high gas velocities and gas recycling. Heat removal from the FT process is achieved by utilizing steam that is generated on the shell side of the reactor. However, this mechanism is not very effective as it results in axial and radial temperature profiles in the tubes.

Typical industrial FTS processes with fixed-bed reactors normally produce complex mixtures consisting of hydrocarbons ranging from methane to wax. For the reasons of reducing pressure drop and facilitating heat removal, catalyst particles of a few millimeters in size are generally needed to be used in fixed-bed reactors, contributing to the existence of intra-particle pore-diffusion limitations. As a result of diffusion limitations and capillary condensation, the catalyst pores are often filled with a stagnant phase formed by the heavy waxy products.

2.6.2 Fluidized Reactor

Fluidized beds generally consist of two phases (gas and solid) and have two types, circulating and fixed. The distinguishing difference between the two types of reactors is that in the fixed fluidized bed reactor (FFD) the catalyst bed remains stationary and the gases pass upward through the bed while in the circulating fluidized bed reactor (CFB) the catalyst is entrained in the fast moving gas stream.

A commercial utilizing FFD reactor technology plant was constructed by Carthage Hydrocol in the 1950's at Brownsville, Texas. This reactor was 18 m high and 4 m in diameter with a nominal capacity of 180,000 tons per year. In this type

of reactor the reaction heat is removed by vertical bundles of cooling tubes submersed in the bed. However this plant was later shut down in 1956 because of technical and economic problem reasons. In a CFB reactor, a fine catalyst bed (40-150 mm diameter) is moved by a high velocity (1–2 m/s) gas stream through a riser reactor. The catalyst is separated from the effluent by cyclones and is then returned to the reactor inlet. Two cooling zones in the riser are used to remove the reaction heat. The improved version of this CFB reactor was named a Synthol reactor at Sasol. The main disadvantage of the two fluidized bed reactors is that should any poison enter the reactor the entire catalyst bed is poisoned whereas in the fixed bed tubular reactor, the poison is adsorbed over the surface of the catalyst leaving the rest of the bed completely [74].

The fixed fluidized bed Sasol advanced Synthol reactor has replaced the circulating fluidized bed Synthol reactor. Gas is introduced through a distributor and bubbles up through the catalyst bed. Heat is removed by an internal heat exchanger immersed in the catalyst bed. These new reactors are half the cost and size of the circulating reactors for the same capacity. They also have better thermal efficiency with a less severe temperature gradient and a lower pressure drop across the reactor. Operating costs are considerably lower and there is greater process flexibility (in terms of product distribution) and the possibility for scale-up to 20,000 BPD [75]. Process conditions in the fixed fluidized bed reactors are similar to those established in the Synthol reactors.

2.6.3 Slurry Bubble Column Reactor

The slurry bed reactor was first operated during the Second World War and up to the late 1970's by Kolbel and co-workers. Sasol's involvement in the development of slurry reactors dates back to the early 1980's, while it was on a small scale. A commercial-scale slurry reactor (5 m diameter and 22 m high) was instructed in May 1993 at Sasol and this reactor has been operated successfully since that time. In these 3-phase reactors syngas is distributed from the bottom and it rises through the slurry that consists of a high thermal capacity liquid (primarily the FT wax product), with the catalyst particles suspended in it. As FTS proceeds with this reactor, the heavy hydrocarbon products form part of the slurry phase while the lighter gaseous products and water diffuse throughout the gas bubbles and then to the gas outlet [76].

Compared with fixed bed reactors that have a tendency of evolving hot spots in the catalyst bed, hot spots are non-existent in slurry phase because of the blending nature of the slurry and controlled slurry mixing. Therefore, the slurry phase is sufficiently well mixed to give an isothermal operation, giving a very efficient heat transfer and uniform temperature. It has been calculated that the heat transfer coefficient for the cooling surfaces in a slurry phase reactor are five times higher than those for fixed bed reactors. Furthermore, the average synthesis temperature can be higher than that used in a fixed bed reactor without the risk of catalyst degradation resulting in higher CO conversions.

Another reactor design is the low-temperature slurry reactor, which has been designed since Kolbel's pioneering work in the 1950s [77, 78]. Slurry bed reactors are three phase reactors consisting of a solid catalyst suspended and dispersed in a high thermal capacity liquid (primarily the FT wax product). Syngas is bubbled through the liquid phase achieving excellent contact with catalyst while keeping the catalyst particles dispersed. Slurry reactors are optimized at low temperatures for high FT wax production with low methane production. Relative to the fluidized bed reactors, the slurry reactors offer the advantages of better temperature control, lower catalyst loading, and significantly lower catalyst attrition rates. The improved isothermal conditions in slurry bed reactors allows for higher average reactor temperatures leading to higher conversions to products. Slurry bed reactors also cost 75% less than the much more complex tubular fixed bed reactors. These reactors have only recently been put into commercial FT production primarily because one of the technical barriers, which required extensive development, was trustworthy catalyst separation from the FT waxes.

The type of catalyst to be used in a reactor is very important to specify for reactor design and operation, since different catalysts will behave differently. For Fe catalysts, substantial tail gas (e.g., recycle ratio 2:1) is needed to supply due to limited conversion causing by water inhibition. For Co catalysts, no water inhibition occurs and the conversion per pass can be higher. Furthermore, the selectivity is strongly dependent on the partial pressures of CO and H_2. A sufficiently high CO

partial pressure, even at the catalyst bed end, should be maintained in order to avoid excessive methane formation.

CHAPTER III
EXPERIMENTAL PROCEDURES

3.1 Material and Reagents

3.1.1 Preparation of Ruthenium Promoted Cobalt Catalysts

The starting materials were Cobalt (II) nitrate hexahydrate {$Co(NO_3)_2 \cdot 6H_2O$ ≥98%, A.R. Grade, Kanto chemical Co.}, Ruthenium(III) nitrate {$Ru(NO_3)_3$, A.R. Grade, Tanaka Noble Metal Co., metal: 100 g/L}, Citric acid {CA, A.R. Grade, Sigma-Aldrich Co.}, 28 wt% of ammonia water {Kanto chemical Co.} and Silica {Q-50, Fuji Silysia Chemical Company, surface area: 78.67 m^2/g, pore volume: 1.055 ml/g}

3.1.2 Preparation of Iron-Based Catalysts

Iron(III) nitrate Nonahydrate {$Fe(NO_3)_3 \cdot 9H_2O$, A.R. Grade, Kanto chemical Co.}, Copper (II) nitrate trihydrate {$Cu(NO_3)_2 \cdot 3H_2O$, A.R. Grade, Kanto chemical Co.}, Potassium Nitrate {KNO_3, A.R. Grade, Kanto chemical Co.}, Citric acid {CA, A.R. Grade, Sigma-Aldrich Co.} and 28 wt% of ammonia water {Kanto chemical Co.} were used as the starting materials

3.2 Catalyst Preparation and Characterization

3.2.1 Preparation of Ruthenium Promoted Cobalt Catalysts

The catalysts containing 10 wt% cobalt and 1 wt% ruthenium were prepared by coimpregnation according to the similar method reported in the literatures [6] on a commercially available silica gel (Q-50), $Co(NO_3)_2 \cdot 6H_2O$, $Ru(NO_3)_3$ solution and

citric acid were used as raw materials. The nitrate compounds are noted as N and citric acid is noted as CA. The cobalt nitrate, ruthenium nitrate and CA were first dissolved in 100 ml of distilled water according to different CA/N molar ratios of 0.15, 0.2, 0.25, 0.3, 0.35 and 0.4, denoted as 0.15RuCo, 0.2RuCo, 0.25RuCo, 0.3RuCo, 0.35RuCo and 0.4RuCo, respectively. The solutions were adjusted by 28 wt% of ammonia water to reach a pH value of 7. Stirring and refluxing at 80 °C for 2 h ensured the CA completely chelated with the metal ions. Subsequently, the neutralized solution was evaporated and condensed at 70 °C on a hot plate with continuous stirring. The catalysts were prepared by impregnation of this condensed solution to silica of 5 g. The obtained catalyst precursors were dried in air at 120 °C for 12 h and then calcined in 80 ml/min flow of argon from room temperature to 400 °C with a ramping rate of 2 °C/min for 3 h, subsequently passivated by 1% oxygen in the argon at room temperature for 4 h. After passivation, the catalysts were directly used for FTS without H_2 reduction.

Figure 3.1 Catalyst calcination apparatus

As a reference catalyst, the air combustion–reduction catalyst $M_{air\text{-}reduction}$ refers to the catalyst prepared by the similar autocombustion method with M metal salt and citric acid (M is Co, Ru or RuCo). The differences are that the catalysts were obtained by calcination in air at 400 °C for 3 h and then reduction at 400 °C for 10 h in H_2. For comparison, conventional impregnated catalysts (denoted as M_N, where M was the loaded metal Co, Ru or RuCo) with 10 wt% cobalt and/or 1 wt% ruthenium were also prepared. The catalysts were calcined in air at 400 °C for 3 h and then reduced in H_2 at 400 °C for 10 h. All of the catalysts were passivated by 1% oxygen in argon at room temperature for 4 h.

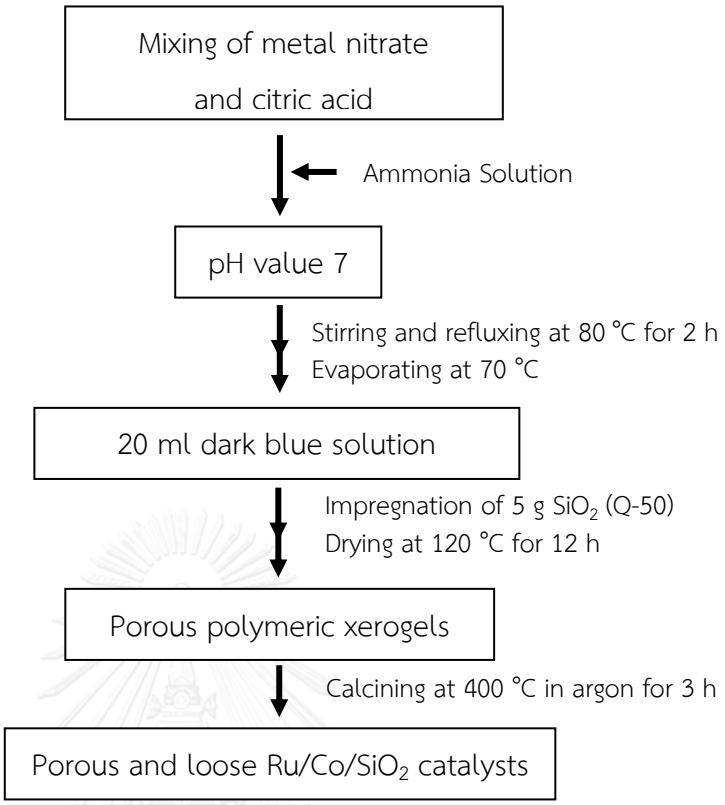

Figure 3.2 Schematic flow chart of the catalysts preparation by autocombustion method

3.2.2 Preparation of Iron-Based Catalysts

The iron-based catalysts were prepared by the sol–gel autocombustion method according to the similar method reported in the literatures [70]. The nitrate compounds are noted as N and citric acid is noted as CA. The mixed aqueous solutions of $Fe(NO_3)_3 \cdot 9H_2O$, $Cu(NO_3)_2 \cdot 3H_2O$ and KNO_3 with molar ratio of Fe:Cu:K was 200:30:5 and CA were first dissolved in the distilled water according to different CA/N molar ratios of 0.1, 0.3, 0.5 and 1, denoted as 0.1Fe-Cu-K, 0.3Fe-Cu-K, 0.5Fe-Cu-K and 1Fe-Cu-K. The solutions were adjusted by 28 wt% of ammonia water to reach a pH value of 7. Stirring and refluxing at 80 °C for 2 h ensured the CA completely chelated

with the metal ions. Subsequently, the neutralized solution was evaporated at 70 °C on a hot plate with continuous stirring. The obtained catalyst precursors were dried in air at 120 °C until porous polymeric xerogels was obtained and then calcined in 80 ml/min flow of argon from room temperature to 500 °C with ramping rate 1.5 °C/min for 5 h. After calcinations, the catalysts were directly used for FTS without further reduction.

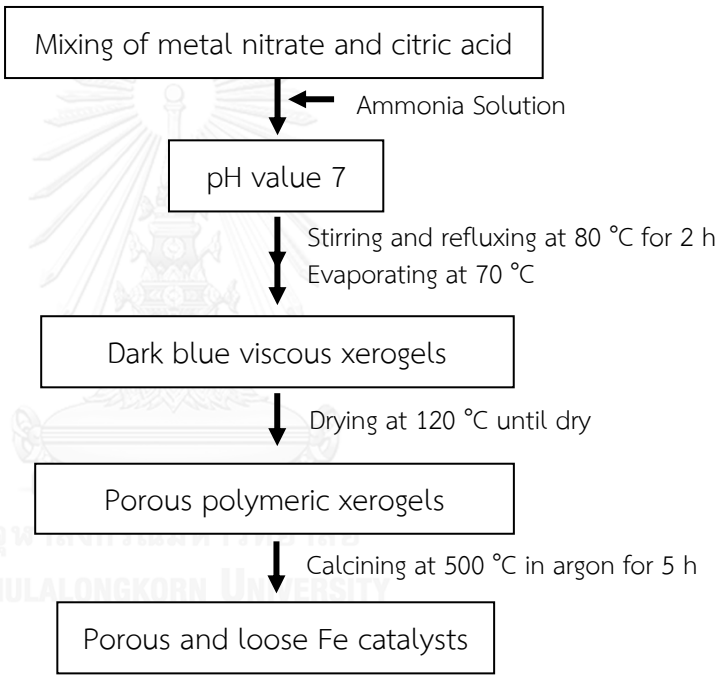

Figure 3.3 Schematic flow chart of the catalysts preparation by sol-gel autocombustion method

For comparison, the iron-base catalyst was also prepared by the co-precipitated method. A solution containing $Fe(NO_3)_3 \cdot 9H_2O$, $Cu(NO_3)_2 \cdot 3H_2O$ and KNO_3 with molar ratio of Fe:Cu:K was 200:30:5 was introduced into the distilled water. The 28 wt% ammonia water was added simultaneously to maintain the pH at

a constant value of 8. After precipitation, the precipitate was filtered. The final product was dried further in air for 12 h at 120 ℃ and then calcined in air at 500 ℃ for 5 h. After calcinations, the catalyst was in situ reduced in H_2/CO flow at 300 ℃ for 10 h, denoted as Fe-Cu-K.

3.2.3 Catalyst Characterization

3.2.3.1 Thermogravimetic and Differential Thermal Analysis (TG/DTA)

The behavior of the autocombustion process was characterized by Thermogravimetic and differential thermal analyses (DTA/TGA-60, Shimadzu) at a heating rate of 10 ℃/min from room temperature to 800 ℃ under a nitrogen atmosphere.

Figure 3.4 Thermogravimetic and differential thermal analysis (DTA/TGA-60, Shimadzu)

3.2.3.2 X-ray Diffraction (XRD)

X-ray diffraction (XRD) patterns of the prepared catalysts were measured using a Rigaku RINT 2200 X-ray powder diffractometer with a monochromatic Cu Kα radiation source at 40 kV and 40 mA in the 2θ range of 10–80 degrees. The average crystalline sizes of the powders were calculated by the Scherrer equation.

Figure 3.5 X-ray Diffractrometer (XRD, RINT 2200, Rigaku. Co.)

3.2.3.3 Brunauer-Emmett-Teller (BET)

The pore structures of the catalysts were determined by N_2 physisorption using a NOVA 2200e apparatus. The samples were degassed at 200 °C for 2 h before the analysis. The specific surface area (S) was obtained by the BET method. The total pore volume (V) was calculated by the single point method and the average pore size was achieved by 4V/S.

Figure 3.6 N_2 physisorption (NOVA 2200e)

3.2.3.4 Hydrogen Temperature-Programmed Reduction (H_2-TPR)

The reduction behaviors were studied by hydrogen temperature-programmed reduction (H_2-TPR, BELCAT-B-TT). Before reduction, the catalysts were heated at 150 °C for 2 h in argon flow. After that, the temperature was cooled down to 50 °C. Then, 5% H_2–Ar mixture gas with a flow rate of 30 cm^3/min was passed through the catalysts. The temperature was linearly raised from 50 °C to 800 °C at a heating rate of 5.0 °C/min. The effluent gas was analyzed using a thermal conductivity detector (TCD).

Figure 3.7 Hydrogen temperature-programmed reduction (H_2-TPR, BELCAT-B-TT)

Figure 3.8 Scanning electron microscopy with X-ray microanalysis (SEM-EDX, JEOL, JSM-6360LV)

3.2.3.5 Scanning Electron Microscopy with X-ray Microanalysis (SEM-EDX)

The determination of the metal content in the catalyst was carried out using a scanning electron microscope equipped with an energy-diffusive X-ray (EDX) spectroscopy attachment (SEM-EDX, JEOL JSM-6360LV).

3.2.3.6 X-ray Photoelectron Spectroscopy (XPS)

X-ray photoelectron spectroscopy (XPS) study was conducted to study the chemical composition and oxidation state of catalyst surfaces. Spectra are recorded on a Thermo ESCALAB 250 Xi spectrometer equipped a monochromatized Al Kα radiation (1486.6 eV). The C_{1s} line at 284.5 eV was used as a reference to correct the binding energies for all catalysts for possible charging effects.

3.3 Fischer–Tropsch Synthesis Tests

3.3.1 Fischer–Tropsch Synthesis Tests for Ruthenium Promoted Cobalt Catalysts

The FTS performance of the catalysts was tested in a semibatch slurry-phase reactor with an inner volume of 80 ml. 1 g of passivated catalyst was ground to fine particles in 20 ml of n-hexadecane, and then the mixture was transferred into the reactor. Syngas with a H_2/CO molar ratio of 2 was used as a reactant and 3% Ar was used as an inner standard. During the reaction, the effluent gas from the reactor was analyzed by online gas chromatography. A thermal conductivity detector (TCD) was used to analyze the gaseous products (CO, CO_2, and CH_4). Light hydrocarbons (C_1–C_5) were online analyzed using a flame ionization detector (FID) with a Porapak-Q column. The liquid products collected in a dry-ice trap and hydrocarbons dissolved

in the solvent were combined and all of them were analyzed using a FID with a silicone SE-30 column. The FTS reaction conditions were: H_2/CO = 2, T = 240 °C, P (total) = 1.0 MPa, and W/F = 10 g•h/mol, where W is the weight of the catalyst and F is total syngas flow rate (including H_2, CO and 3% Ar).

3.3.2 Fischer–Tropsch Synthesis Tests for Iron-Based Catalysts

The reaction performance of the catalysts in FTS was carried out in a semibatch slurry-phase reactor with an inner volume of 80 ml. 1 g of the calcined catalyst was transferred to a mortar filled with 20 ml PAO as liquid medium, where it was ground to fine particles and were then loaded in the reactor. A mixture of H_2 and CO with a H_2/CO molar ratio of 1 was used as syngas reactant and 3% Ar was used as an inner standard. Before the reaction, reactant gas was used to clean the calcined catalyst for 1 hour at same temperature used in FTS. During the reaction, the effluent gas from the reactor was analyzed by online gas chromatography. A thermal conductivity detector (TCD) was used to analyze gaseous products (CO, CO_2, and CH_4). Light hydrocarbons (C_1-C_5) were online analyzed by a flame ionization detector (FID) with a Porapak-Q column. The liquid products collected in a dry-ice trap and hydrocarbons dissolved in the solvent were combined and all of them were analyzed by FID with a silicone SE-30 column. The FTS reaction conditions were P (total) = 1.0 MPa, T = 300 °C, W/F (CO + H_2 + 3% Ar) = 10 g•h/mol.

Figure 3.9 The Fischer-Tropsch synthesis unit

Figure 3.10 Gas chromatography-Flame ionization detector (GC-FID) with a silicone SE-30 column for liquid products analysis

CHAPTER IV
RESULTS AND DISCUSSION

The study in this chapter is divided into two parts. The first part describes characteristics and catalytic activity of ruthenium (Ru) promoted Co/SiO_2 catalyst prepared by the autocombustion method with various different reductant types and the reductant content. The as-synthesized catalysts were compared with the conventional impregnated catalysts reduced in H_2. The second part of this study is synthesis the iron-based catalyst with the different amount of citric acid that used as a reductant. It was also compared with the conventional co-precipitation catalyst that reduced in syngas with CO/H_2 molar ratio of 1.

4.1 The Ru Promoted Co/SiO_2 Catalysts

4.1.1 Evolution of Ru Promoted Co/SiO_2 Catalysts during the Autocombustion Process

The series of Ru promoted Co/SiO_2 FTS catalysts were prepared by the autocombustion method using cobalt and ruthenium nitrate as the oxidants and citric acid as the reductant. After the impregnation of the precursors over SiO_2 (Q-50), dry samples were characterized by Thermogravimetric and differential thermal analysis (TG/DTA) to elucidate the evolution of the Ru promoted Co/SiO_2 catalyst during the autocombustion process. The TG/DTA results of the dry samples prepared with different reductant content (molar ratio of citric acid to nitrate: CA/N) are shown in Figure 4.1.

The DTA curves of the samples exhibited one endothermic peak and two exothermic peaks. The endothermic peak below 100 ℃ could be ascribed to the removal of adsorbed water. The two exothermal peaks at about 200 and 270 ℃ were assigned to the redox reaction of nitrate with citric acid, meanwhile the TG plots decreased deeply. During this process, nitrate and citric acid were decomposed, and a large amount of gases such as H_2, CO, H_2O, CH_4, NO, CO_2, NH_3 and NO_2 were released. The formed H_2, CO and CH_4 acted as the reductants to reduce the metal oxides to metallic Co and Ru. Ru might be reduced first because of lower reduction temperature. The reduced Ru could then induce the reduction of cobalt oxide. After the temperature become higher than 300 ℃, the weight losses of the catalysts were changed smally.

The study of catalysts with different citric acid content, the result is clearly that both decomposition and redox reaction of nitrate and citric acid took place in a low rate at low CA/N ratio (0.15-0.3). With the increase of CA/N ratio, the intensity of the exothermic peak increased, indicating that the combustion process occurred more severely. Moreover, in the temperature regions of 180-250 ℃, the weight loss increased with the increasing of citric acid contents. It needs to note that the weight losses in 0.35RuCo and 0.4RuCo are much smaller than that in 0.3RuCo. This is because excessive citric acid might result in obvious carbon deposition over the catalysts. The deposition of carbon species could decrease the weight loss of the catalysts.

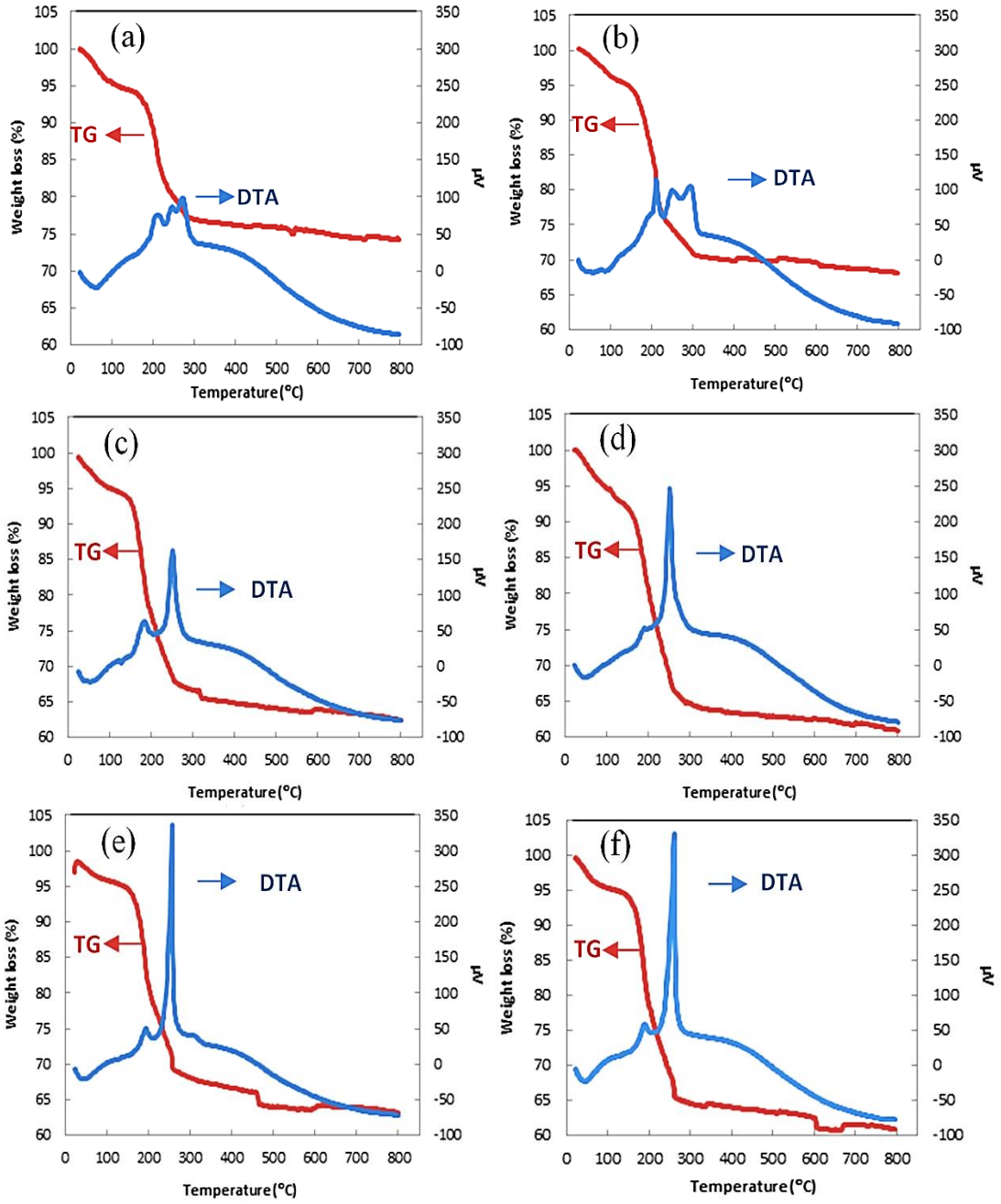

Figure 4.1 TG/DTA curves of Ru-promoted Co catalysts with different CA/N ratios: (a) 0.15RuCo, (b) 0.2RuCo, (c) 0.25RuCo, (d) 0.3RuCo, (e) 0.35RuCo and (f) 0.4RuCo

4.1.2 Physical and Chemical Properties of Ru Promoted Co/SiO_2 Catalysts Synthesized by the Autocombustion Method

4.1.2.1 Crystal Phase Analysis of As-synthesized Catalysts

The XRD patterns of Ru promoted Co/SiO_2 catalysts prepared by different method are presented in Figure 4.2a. The XRD spectra of Co and Ru monometal catalysts were also characterized and the results were shown in Figure 4.2b and Figure 4.2c, respectively. It can be seen that the catalyst prepared by Ru promoted Co/SiO_2 autocombustion catalyst (0.3RuCo) exhibited weak peaks for metallic Co and SiO_2. There is no diffraction peaks for cobalt oxides identified in this catalyst because the most of cobalt oxides were reduced to metallic Co and the formed Co were well dispersed. The air-reduction catalyst refers to the catalyst prepared by the similar autocombustion method. The differences are that the catalysts were obtained by calcination in air at 400 °C for 3 h and then reduction at 400 °C for 10 h in H_2. For Ru promoted Co catalysts prepared by air combustion-reduction ($0.3RuCo_{air\text{-}reduction}$) and conventional ($RuCo_N$) methods, both SiO_2 and metallic Co crystals were identified, but the crystalline peaks of Co shows much sharper than those of the autocombustion catalyst. It could be concluded that the catalyst prepared by the autocombustion method exhibited a higher Co dispersion than those prepared by the air combustion-reduction and conventional methods.

The results of cobalt catalyst without ruthenium promotion (0.3Co) are portrayed in Figure 4.2b. The weak diffraction peaks at 2θ = 44.05° for metallic cobalt

crystalline of the as-synthesized catalysts were identified and the peak intensity for metallic cobalt crystalline in 0.3Co is weaker than that in 0.3RuCo. Furthermore, CoO crystalline was also observed in 0.3Co catalyst. These results indicate that only part of cobalt was reduced at low reduction content (CA/N=0.3) without ruthenium promotion. Therefore, ruthenium played an important role in the reduction of cobalt during the autocombustion process. Furthermore, no obvious diffraction peaks except for SiO_2 were found in 0.3Ru catalyst. This result was probably due to the low content and well dispersion of Ru in the catalyst.

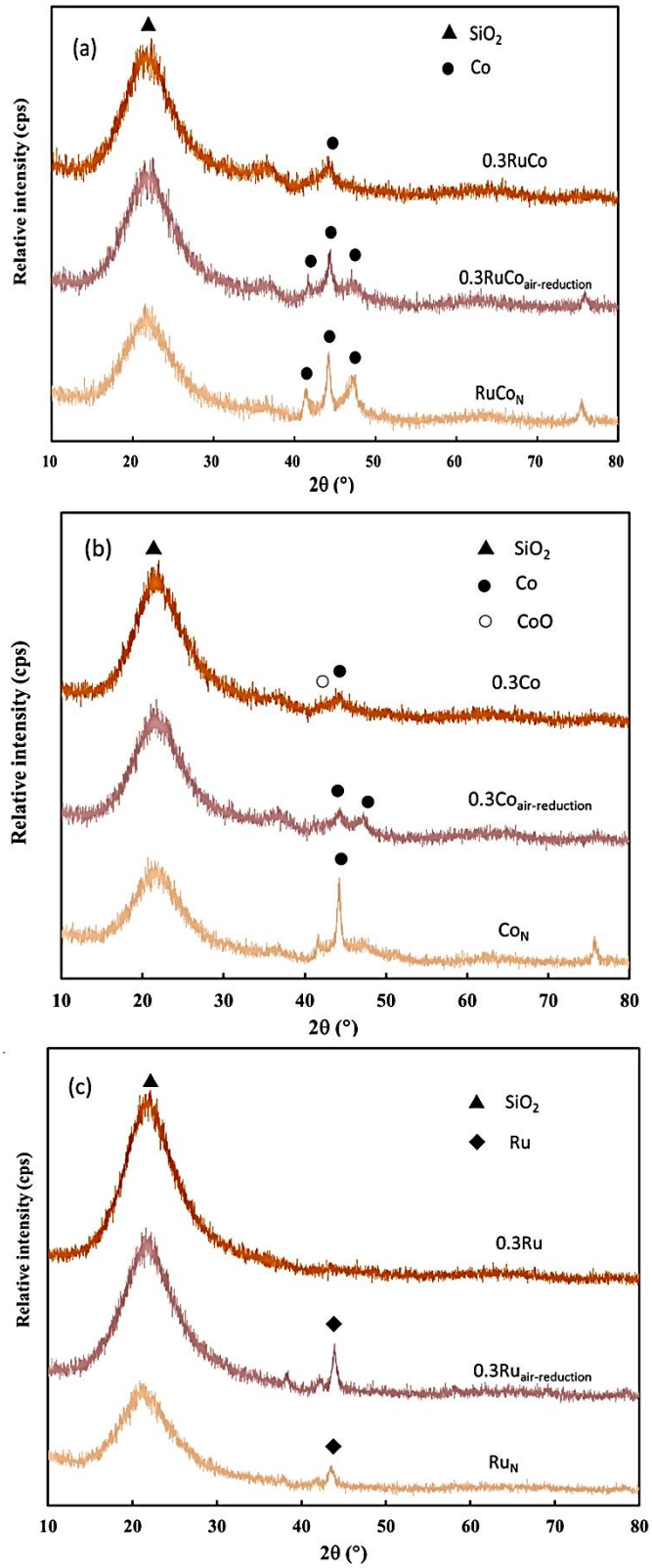

Figure 4.2 X-ray diffraction patterns of the catalysts prepared by different methods: (a) RuCo, (b) Co, (c) Ru catalysts

The effect of CA/N on the reduction and dispersion of cobalt was also studied by XRD, and the results are presented in Figure 4.3 and Table 4.1. The narrow and intense diffraction peaks of 0.15RuCo at 36.46° and 42.32° are indexed to CoO phase, showing that the major phase of this catalyst is CoO. It means that the amount of citric acid was not enough to reduce Co_3O_4 completely and some CoO was left. With the increase of CA/N in the precursors, the diffraction peaks of CoO at 36.46° and 42.32° gradually decreased while the diffraction peaks of metallic Co at 44.04° became stronger. When CA/N increased to 0.3, pure metallic Co was obtained. However, further increasing CA/N to 0.4, small and board peaks for metallic Co was observed. This result indicated that the metallic Co sites were relative small and well-dispersed at a high reductant content.

During the autocombustion process, citric acid was decomposed into a large amount of gases such as H_2, H_2O, CO, CH_4 and CO_2, which could reduce the cobalt oxides to metallic Co [6] . With the increase of citric acid content, more H_2, CO and CH_4 were formed, and thus more cobalt oxides were reduced to metallic Co. In the previous work [6]. Co/SiO_2 catalyst was synthesized by the autocombustion method using citric acid as a reductant and burnt under Ar atmosphere, but the highest activity was achieved at a very high reductant content (CA/N=1). In this work, the smaller amount of reductant (CA/N=0.3) could reduce the cobalt oxides completely. This result further proved that the addition of Ru promoted the reduction of cobalt.

Furthermore, ruthenium also acted as a structural promoter to raise the dispersion of cobalt particles and decrease the average cobalt cluster sizes [2].

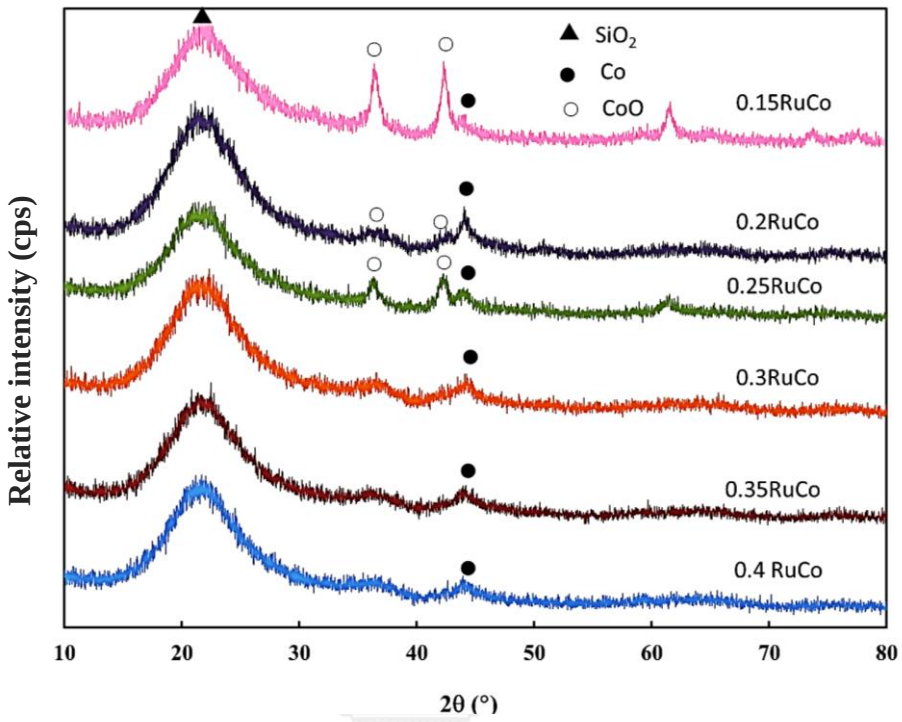

Figure 4.3 The X-ray diffraction patterns of the as-synthesized catalysts with different content of reductant

4.1.2.2 Pore Structure and Elemental Composition Analysis

The pore structure parameters of the as-synthesized catalysts are shown in Table 4.1. The crystallite sizes of the as-synthesized catalysts were also calculated by the Scherrer formula and the values are reported in Table 4.1. The BET surface area of support silica (Q-50) was 79 m^2/g whereas the surface area of the as-synthesized catalyst 0.3RuCo was 90 m^2/g. The increase in BET surface area after the autocombustion was mainly derived from some Co nanoparticles loaded in the pores of support. With the increase of CA/N molar ratio, the BET surface area of the as-synthesized catalyst first increased, reached a maximum at 0.3RuCo, and then

decreased. This is because more reductant led to smaller Co particle sizes, which could improve the BET surface area. However, excessive reductant could result in oversupply of the carbonic residues, and cause the decrease in the surface areas. For 0.4RuCo catalyst, although it had the smallest Co crystalline size, its surface area was limited to 74 m^2/g due to the accumulation of excessive carbonic residues.

The metal contents of the catalysts prepared by the autocombustion and conventional impregnation methods were measured by scanning electron microscopy (SEM) with EDX and the results are shown in Table 4.1. The contents of Ru and Co prepared by the autocombustion method are close to the desired values. But the content of Co in conventional prepared catalyst is much higher than the loaded contents. This result might be attributed to the fact that more Co was impregnated on the external surface of the catalysts.

Table 4.1 Physical and chemical parameters of the catalysts

Catalysts	Surface areas[a] (m^2/g)	Pore volume[a] (cm^3/g)	Pore diameter[a] (nm)	Crystallite size[b] (nm)	EDX (wt%) Co	Ru
0.15RuCo	80	0.68	21	11.3[c]	11.0	1.2
0.2RuCo	79	0.91	20	10.0	9.9	0.7
0.25RuCo	77	1.32	21	9.1	9.3	0.7
0.3RuCo	90	1.19	37	6.7	10.6	1.3
0.35RuCo	81	0.95	32	6.0	10.3	1.0
0.4RuCo	74	1.05	21	5.0	10.2	1.3
$RuCo_N$	74	1.08	21	15.5	12.1	0.9
Co_N	83	0.70	21	13.7	12.8	-

[a] Determined by N_2 adsorption method.

[b] Calculated by the Scherrer formula, using the peak at 2θ = 44.05°.

[c] CoO crystalline size.

4.1.2.3 X-ray Photoelectron Spectroscopy of RuCo Catalysts

XPS measurement was carried out in order to get more quantitative information about the surface structure of the Ru promoted Co catalysts. Figure 4.4 shows the Co 2p XPS spectra of the as-synthesized catalysts after calcination and the peak binding energy of them are listed in Table 4.2. The XPS data of Co and Ru peak for the 0.3RuCo catalysts are also presented in Figure 4.5. The binding energy is

determined from the Co $2p_{3/2}$ and Ru $3d_{5/2}$ peaks at ≈781.08 and ≈283.88 eV, respectively. These energy values for cobalt oxide are in agreement with other works [44, 61]. There are a slightly different in the shapes and energy positions of the photoelectron peaks for all as-synthesized catalysts as shown in Figure 4.4a. For Ru promoted Co catalysts prepared by air combustion-reduction ($0.3RuCo_{\text{air-reduction}}$) and conventional ($RuCo_N$) methods, the binding energy of them are determined from the Co $2p_{3/2}$ and Co $2p_{1/2}$ at ≈779.08 eV and ≈795.4 eV, respectively. These energy values for metallic cobalt are in agreement with other works [44, 61]. Figure 4.4b presents the Co 2p XPS spectra of the reduced catalysts ($RuCo_N$) and the as-synthesized catalysts. In the case of $0.3RuCo_{\text{air-reduction}}$ and $RuCo_N$, there is a shift to lower binding energy in the energy position of the Co 2p peaks relative to the spectrum of the as-synthesized catalyst (0.3RuCo). It would seem to suggest that the cobalt oxide of the as-synthesized catalysts were presented on the surface.

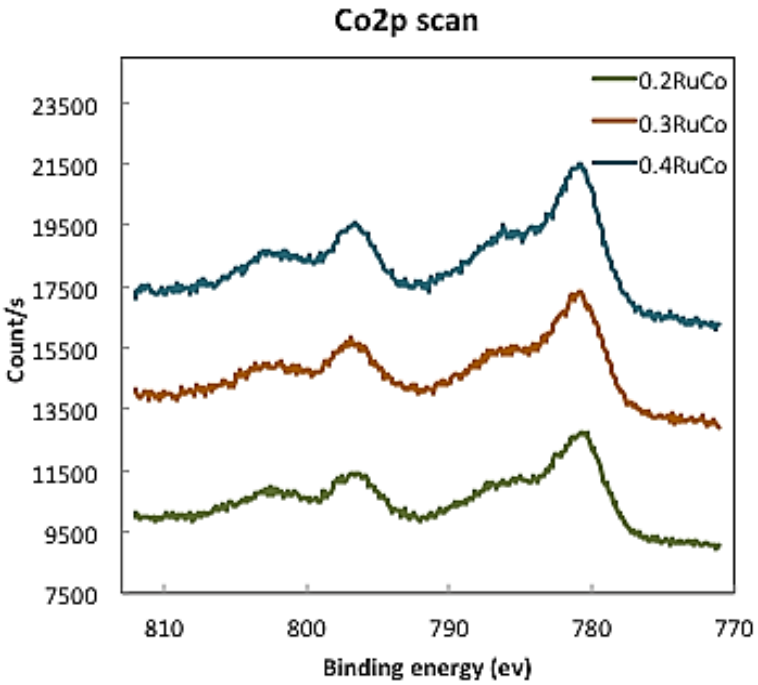

(a)

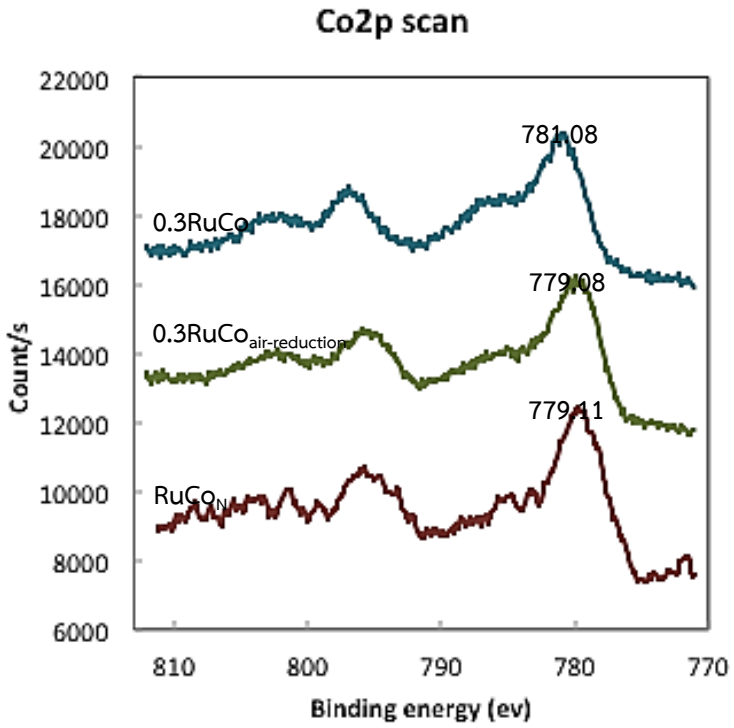

(b)

Figure 4.4 XPS Co 2p spectra of the Ru-promoted Co catalysts: (a) the autocombustion catalysts, (b) the catalysts prepared by different methods

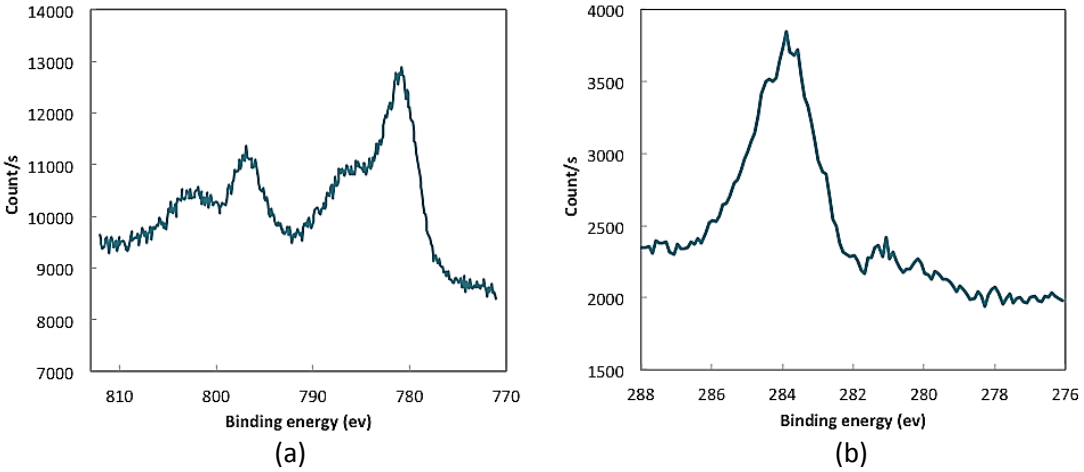

Figure 4.5 X-ray photon spectra for chemical analysis of the 0.3RuCo catalysts: (a) Co and (b) Ru

Table 4.2 Summarized results of XPS analysis on the Ru-promoted Co catalysts.

Catalysts	Peak binding energy (eV)	
	Co $2p_{3/2}$	Co $2p_{1/2}$
0.15RuCo	781.01	796.52
0.2RuCo	780.78	796.98
0.25RuCo	781.08	796.58
0.3RuCo	781.08	796.58
0.35RuCo	781.38	796.48
0.4RuCo	781.28	796.78
$RuCo_N$	779.08	795.48
$0.3RuCo_{air\text{-}reduction}$	779.11	795.38

4.1.2.4 Reduction Property of as-synthesized Catalysts

The reduction property of Ru promoted Co catalysts was characterized by H_2 temperature programmed reduction (TPR). For comparison, TPR curves of the monometal catalysts and the catalysts prepared by conventional impregnated method were also measured. The TPR results of different catalysts are shown in Figure 4.6. The reduction of the calcined catalyst (Co_N) can be assigned to a two-step reduction of Co_3O_4 to CoO and then to metallic Co. As a result, for the calcined RuCoN catalyst, adding Ru decreased the reduction temperature of cobalt. The reduction of RuO_2 to metallic Ru usually takes place at a lower temperature than that of Co_3O_4 [5, 62]. It did not exhibit a separate peak in calcined ($RuCo_N$) catalyst and was probably overlapped with the first reduction peak (180 °C) of Co_3O_4. The peak at 250 °C is due to reduction of CoO, which is promoted by Ru *via* hydrogen spillover [63]. For the Ru catalysts prepared by the autocombustion method 0.3Ru, there was nearly no reduction peaks. This result was probably attributed to the fact that the amount of Ru was very low (1 wt%) and most of the Ru was reduced during the autocombustion process. However, for the monometal catalyst 0.3Co, a relative high reduction temperature and a large amount of H_2 consumption are observed. This phenomenon suggested that the reduction of cobalt oxide was more difficult and most of the Co was not reduced in 0.3Co. In the case of 0.3RuCo, the reduction temperature of Co was much lower and the H_2 consumption was much smaller than those of $RuCo_N$ and 0.3Co, demonstrating that most of the cobalt in 0.3RuCo was

reduced during the autocombustion process. These results confirmed that Ru promoted the cobalt reduction during the autocombustion process.

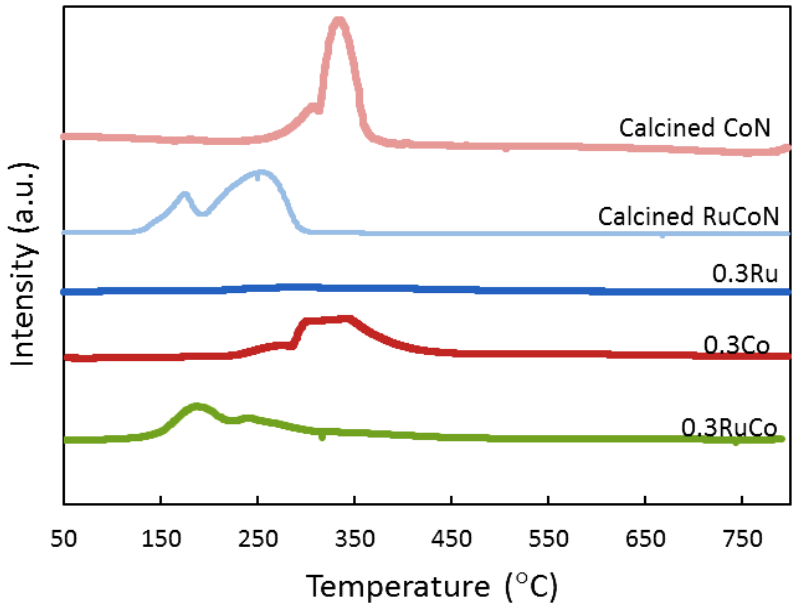

Figure 4.6 TPR profiles of the catalysts prepared by different method

TPR profiles of Ru promoted Co catalysts with different reductant content are compared in Figure 4.7. With an increase in reductant content, the peak for Co reduction (250 °C) decreased gradually and even disappeared at the CA/N ratio of 0.35. This result indicated that the reduction level of cobalt increased with the reductant content. A large amount of H_2 was released from the decomposition of citric acid during the autocombustion process, which could reduce the cobalt oxides to metallic Co. However, excessive reductant could affect in severe residual carbon species in the catalyst. The broad peak at about 350-450 °C in 0.4RuCo catalyst was ascribed to the hydrogenation of residual amorphous carbon.

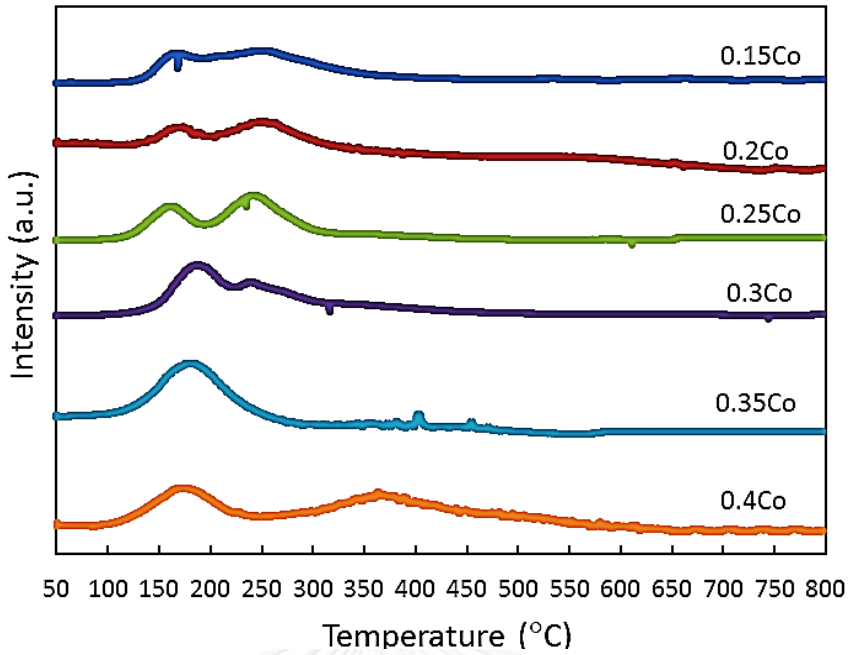

Figure 4.7 TPR profiles of the catalysts with different reductant content

4.1.3 FTS Performances of Ru Promoted Co/SiO_2 Catalysts Prepared by the Autocombustion Method

4.1.3.1 Effect of Ru Promotion on the FTS Performance of the Catalyst

The FTS catalytic activities of the catalysts prepared by different method were measured in a slurry bed reactor under the reaction condition of 240 °C, 1.0 MPa and $H_2/CO=2$. The activity curves and product selectivities are shown in Figure 4.8 and Table 4.3. In this work, the reaction time is five hours and the measured activities were the initial activities. Generally, the initial activity may not correlate well with the steady-state activity. Fortunately, the initial activities of the catalysts are relative stable as shown in Figure 4.8, so we can make the correlation between the structures and performances of the catalysts.

The FTS activities of monometal catalysts prepared by the autocombustion method are very low. The CO conversion of 0.3Co and 0.3Ru were only 0.8 and 1.7%, respectively. The low activity of 0.3Co is mainly attributed to that most of cobalt oxide was not reduced during the autocombustion. Although most of Ru was reduced in 0.3Ru catalyst, the small loading amount as well as the high dispersion of Ru might result in the low activity. The Ru promoted Co/SiO_2 catalyst prepared by the autocombustion method (0.3RuCo) exhibited a high FTS activity with the CO conversion of 41.1%. Furthermore, there was no obvious activity loss in the five hours of reaction time on stream, indicating a high stability of this catalyst as shown in Figure 4.8. It is believed that the promotion of Ru on the reduction and dispersion of Co (Table 4.1 and Figure 4.3) played important roles in the high activity of 0.3RuCo. Ru itself in 0.3RuCo catalyst may also contribute significantly to the high FTS activity by improving Co nature as an effective promoter, as demonstrated by other authors [52, 61].

Table 4.3 The FTS[a] performance of the catalysts prepared by different method

Catalysts	Conversion of CO (%)	Selectivity (%)			α
		CO_2	CH_4	C_{5+}	
0.3RuCo	41.4	3.5	21.1	59.8	0.83
0.3Co	0.8	-	-	-	-
0.3Ru	1.7	-	-	-	-
$0.3RuCo_{air\text{-}reduction}$	60.4	8.5	21.1	64.1	0.82
$0.3Co_{air\text{-}reduction}$	26.5	4.1	14.4	68.3	0.81
$RuCo_N$	45.1	3.4	19.7	60.6	0.77
Co_N	27.7	3.0	25.4	50.4	0.76
Ru_N	8.0	-	-	-	-

[a] The reactions were carried out under the conditions of H_2/CO=2, 240 °C, 1 MPa, W/F (CO, H_2 and 3% Ar) = 10 g·h/mol, and reaction time of 5 h.

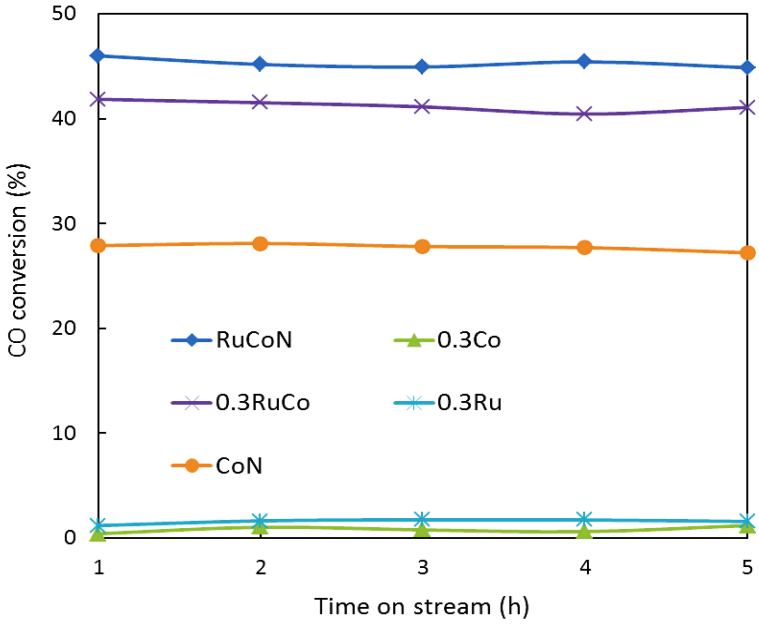

Figure 4.8 Activity curves of the catalysts prepared by different methods (FTS reaction conditions: H_2/CO=2, 240 °C, 1 MPa, W/F (CO, H_2 and 3% Ar) = 10 g•h/mol)

The improvements of FTS catalytic activity by Ru were also found for the catalysts prepared by air combustion-reduction ($0.3RuCo_{air\text{-}reduction}$) and conventional impregnated ($RuCo_N$) methods. It is worthy to note that the CO conversion and hydrocarbon selectivity of 0.3RuCo are similar to those of $RuCo_N$. It can be concluded that the Ru promoted Co catalyst prepared by the autocombustion method can omit the complex and high energy consumed reduction process, and achieved the similar activity and selectivity to the catalyst prepared by the conventional method. Therefore, the surface impregnation autocombustion method may open a new way to prepare metallic catalysts without further reduction, especially the catalysts which were difficult to be reduced at higher temperature.

It needs to be noted that the chain growth factors (α) of the catalysts prepared by the autocombustion method are in the region of 0.81-0.83, which is much smaller than the conventional cobalt catalysts (about 0.88) [42, 43]. There are two possible reasons for these results. One is that the cobalt crystallite sizes prepared by the autocombustion method were much smaller and the finely dispersed metallic crystallites were not suitable for carbon chain growth reaction. The other is that the relative high reaction temperature (240 °C) promoted more methane and less long chain hydrocarbons formation.

4.1.3.2 Effect of Citric acid Contents on the FTS Performance

FTS catalytic activities and selectivities of Ru promoted Co catalysts with different CA/N are presented in Figure 4.9 and Table 4.4. All the catalysts prepared by the autocombustion method exhibited high stable initial activities for the FTS as shown in Figure 4.9. It is clear that 0.15RuCo catalyst exhibited a limited CO conversion as low as 21.4%, which is mainly restricted by its unreduced CoO as shown in Figure 4.3 and Table 4.1. With the increase of CA/N, the content of reduced cobalt increased and the CO conversion generally increased. But oversupplied of CA (0.4RuCo) resulted in the decrease of CO conversion. The small sizes of cobalt crystallines and a lot of carbonic residues accumulated on their surfaces resulted in the low CO conversion. For the 0.4RuCo catalyst, the methane selectivity was high, which may be also due to its small sizes of cobalt crystallines. The finely dispersed

metallic crystallites are not suitable for carbon chain growth and then enhance the methane formation [6].

Table 4.4 The FTS[a] performance of the catalysts with different content of reductant

Catalysts	Conversion of CO (%)	Selectivity (%)			α
		CO_2	CH_4	C_{5+}	
0.15RuCo	21.4	2.8	14.1	72.4	0.89
0.2RuCo	28.1	2.8	17.1	66.6	0.87
0.25RuCo	34.1	2.9	17.3	65.7	0.87
0.3RuCo	41.4	3.5	20.5	59.8	0.83
0.35RuCo	32.7	3.3	20.1	58	0.77
0.4RuCo	28.7	3.2	23.0	57.4	0.77

[a] The reactions were carried out under the conditions of H_2/CO=2, 240 °C, 1 MPa, W/F (CO, H_2 and 3% Ar) = 10 g·h/mol, and reaction time of 5 h.

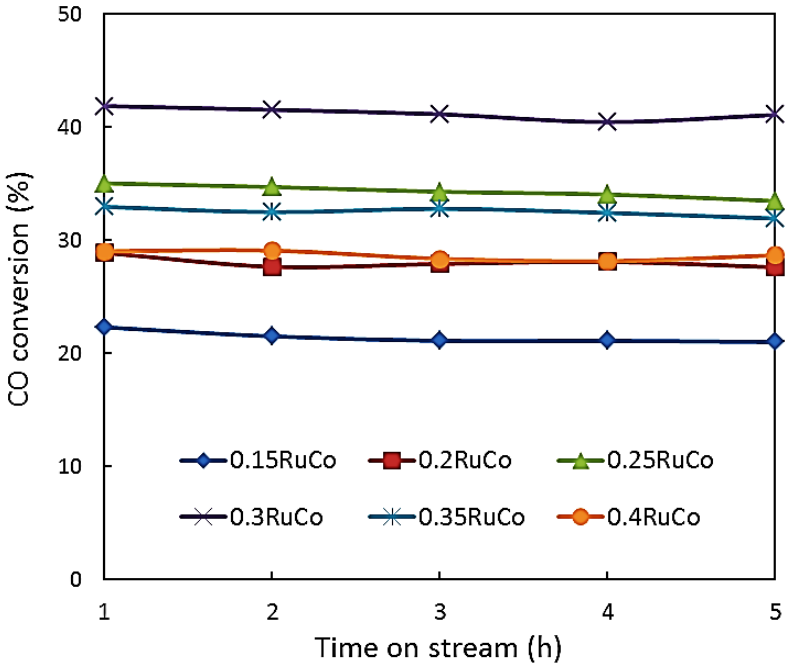

Figure 4.9 Activity curves of the catalysts with different reductant content (FTS reaction conditions: H_2/CO=2, 240 °C, 1 MPa, W/F (CO, H_2 and 3% Ar) = 10 g•h/mol)

4.1.3.3 Effect of Reductant Types on the FTS Performance

In this work, Ru promoted catalysts with various types of organic reductants were also synthesized and tested for the FTS performance. The molar ratio of reductant to nitrate is fixed at 0.3 for all the catalysts. The FTS activities and selectivities of these catalysts are listed in Table 4.5. It can be found that organic reductant types showed remarkable influence on the FTS performance. When citric acid was used as the reductant, the maximum catalytic activity was achieved. The high activity might be due to the high amount of C, H, and O atoms in citric acid molecule, which can release more reducing gases during the autocombustion and improve the reduction of the metals. The sequence of catalytic activity followed the

order of citric acid > formic acid > oxalic acid. Although the catalyst prepared by oxalic acid showed the lowest activity, the lowest methane and the highest C_{5+} selectivities were achieved in this catalyst.

Table 4.5 The FTS[a] performance of the catalysts prepared using different organic reductants

Reductant	Conversion of CO (%)	Selectivity (%)			α
		CO_2	CH_4	C_{5+}	
formic acid	38.7	2.2	19.4	65.0	0.81
oxalic acid	32.8	1.7	15.7	67.9	0.79
citric acid	41.4	3.5	20.5	59.8	0.83

[a] The reactions were carried out under the conditions of H_2/CO=2, 240 °C, 1 MPa, W/F (CO, H_2 and 3% Ar) = 10 g·h/mol, and reaction time of 5 h.

4.2 The Iron-Based Catalysts (Fe-Cu-K)

4.2.1 Crystal Phase Analysis of as-synthesized Catalysts XRD Analysis

X-ray diffractions of the catalysts are shown in Figure 4.10. The crystallite sizes of the as-synthesized catalysts were also calculated by the Scherrer formula and the values are reported in Table 4.6. The as-synthesized catalysts exhibited the mixed of the oxide phases (magnetite, Fe_2O_3) and carbides phases (Fe_2C) as the detectable iron phase, indicating that the autocombustion process completed the conversion of the metal compounds to metal oxides and carbonates without further reduction. No peaks assigned to copper or potassium species were observed on these catalysts, because of their low contents and high dispersion. It was displayed that the Fe_2O_3

and Fe_2C small crystallite size of 0.1Fe-Cu-K was about 263.2 Å and 229.5 Å, respectively. With the increase of the citric acid content in the precursors, crystallite sites were gradually increased to large crystallite sizes. However, when the CA/N molar ratio was further increased to 1, boarder peaks were observed, indicating that the active sites become almost amorphous. The increasing of citric acid contents in starting solution causes more compositional homogeneity of the gel. Because the more citric acid is added to the solution, the more carboxylic groups (-COOH) are generated to chelate Fe^{3+}. As the carbon chains in citrates are decomposed during combustion and calcinations, adjacent Fe^{3+} ions, which are homogeneously distributed throughout the matrix, can more easily and completely come into contact and form crystal lattice. However, using the excess citric acid leads to some carbon residue in the catalyst.

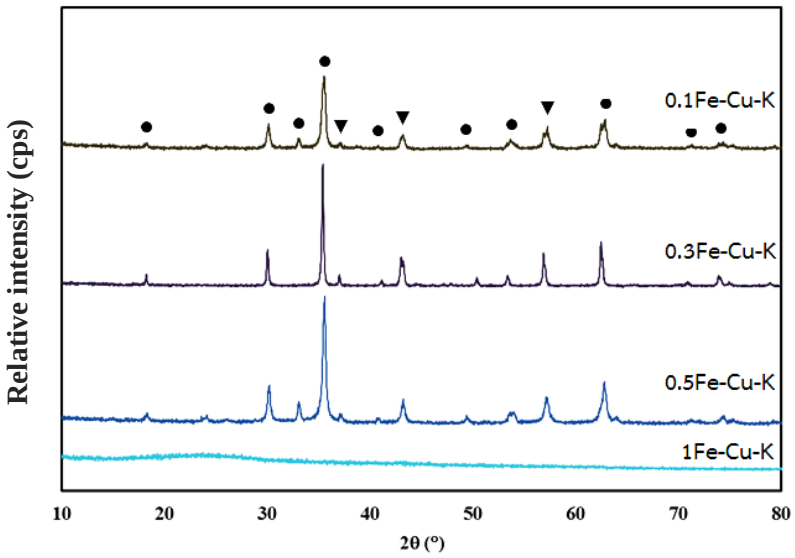

Figure 4.10 The X-ray diffraction of catalysts after calcinations at 500 °C without reduction (▼, Fe_2C; ●, magnetite Fe_2O_3; ■ , Fe)

Table 4.6 The catalytic performance of the catalysts for FTS[a]

Catalysts	Crystallite size[b] (Å)		Conversion of CO (%)	Selectivity (%)	
	Fe_2O_3	Fe_2C		CO_2	CH_4
Fe-Cu-K[c]	-	-	78.2	52.5	7.5
0.1Fe-Cu-K	263.2	229.5	86.3	45.8	5.8
0.3Fe-Cu-K	294.6	256.8	77.1	46.3	5.7
0.5Fe-Cu-K	282.4	252.0	72.8	47.4	6.9
1Fe-Cu-K	-	-	-	-	-

[a] The reaction were carried out under condition of 300 °C, pressure at 1 MPa, 1 g catalyst, W/F ($CO+H_2$ and 3% Ar) = 10 g·mol/h, reaction time 5 hours.

[b] Calculated by Scherrer formula, using the peak at 2θ = 35.5° for Fe_2O_3 and 2θ = 57.1° for Fe_2C.

[c] The co-precipitated catalyst

4.2.2 FTS Performances of Iron-Based Catalysts Prepared by the Autocombustion Method

The as-synthesized iron-based catalyst was applied to FTS reaction to investigate the role of citric acid and promotion adding in the precursor solutions. Table 4.6 shows the catalytic activities of iron-based FTS catalysts over different CA/N molar ratios. The CO conversion as a function of a reaction time is showed in Figure 4.11. Fortunately, the initial activities of the catalysts are relative stable as shown in Figure 4.11A, so we can make the correlation between the structures and

performance of the catalysts. Contrarily, the conventional iron-based catalyst that the CO conversion reached the stable state in the fifth hour of the reaction as presented in Figure 4.11B. These results proved that the autocombustion method could prepare high stability catalysts. According to Table 4.6, the Fe-Cu-K catalyst with CA/N molar ratio at 0.1 exhibited highest CO conversion as high as 86.3% and relative low CO_2 and CH_4 selectivity compared with the other catalysts. With an increase CA/N molar ratio, the CO conversion was decreased. For the oversupply CA catalysts (CA/N =1), had no activity due to the active sites become almost amorphous as demonstrated in XRD result (Figure 4.10). Furthermore, the FTS on iron-base catalysts is accompanied by the water gas shift (WGS) reaction. In this reaction, CO reacts with water, which is generated from FTS, and produces CO_2 and H_2 ($CO+H_2O \leftrightarrow CO_2 + H_2$) [37]. The CO_2 was mainly derived from WGS reaction, and its selectivity hardly changed.

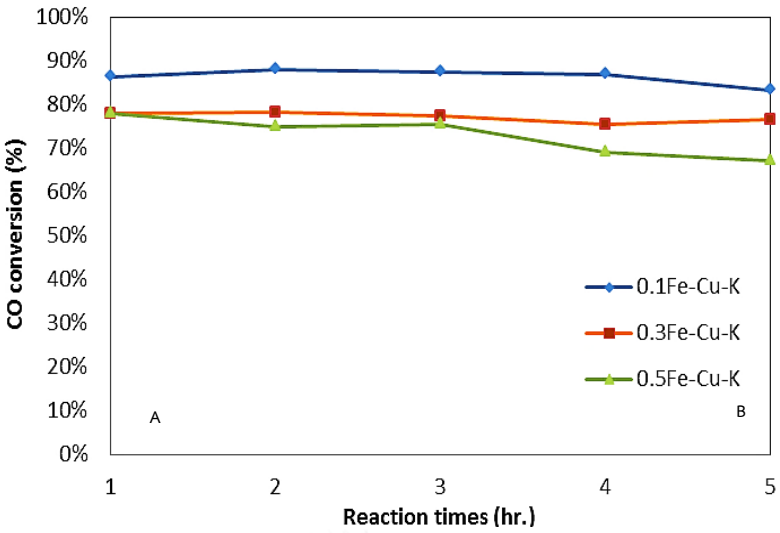

(a)

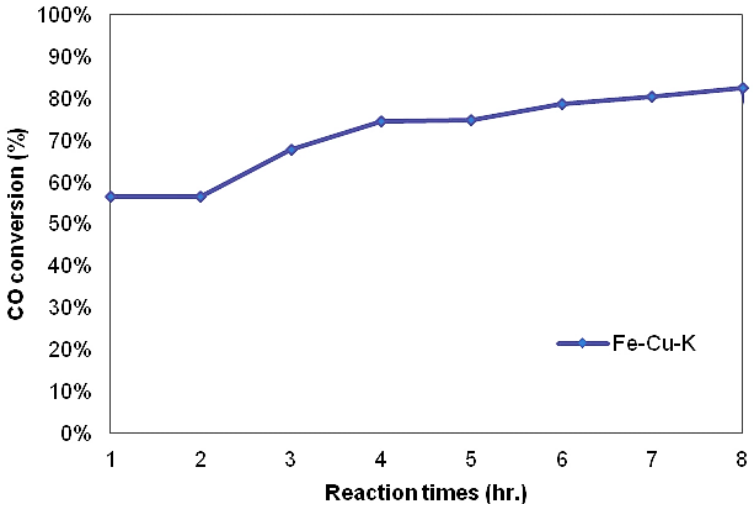

(b)

Figure 4.11 The CO conversion as a function of a reaction time of Fe-Cu-K catalysts

CHAPTER V
CONCLUSIONS AND RECOMMENDATIONS

This work focuses on the development of FTS catalysts with high reduction level were successfully prepared by the autocombustion method using citric acid as a reductant and nitrate ions as oxidants. The as-synthesized catalysts were used directly in Fischer-Tropsch synthesis without further reduction. The effects of ruthenium promoter, citric acid contents, and reductant types in the precursors on the catalyst structures and FTS performances were studied. The crystalline phases, surface areas and reduction behavior of the as-synthesized catalysts also have been investigated using Thermogravimetic/Differential thermal analysis, X-ray diffraction, Nitrogen adsorption–desorption, X-ray photoelectron spectroscopy, Scanning electron microscopy equipped with energy-dispersive X-ray analysis and Hydrogen temperature-programmed reduction. The conclusions are summarized as follows:

5.1 Ru Promoted Co Catalysts

5.1.1 Characterization of Catalysts

The TG/DTA results of the Ru promoted Co/SiO_2 catalysts exhibited the effect of reductant content on the combustion process. The intensity of the exothermic peak increased when the citric acid content was increased, indicating that the combustion process occurred more severely. The finding from XRD patterns indicated that most of the cobalt oxides were reduced to metallic Co and the formed Co were well dispersed. When the CA/N molar ratio was increased, the diffraction peaks of

CoO gradually decreased and the diffraction peaks of metallic Co became stronger, indicating that the cobalt oxide was more reduced at high reductant content. Furthermore, BET surface area of catalysts was increased after the autocombustion. With the increase of reductant content, the BET surface area of the as-synthesized catalyst first increased, reached a maximum at 0.3RuCo, and then decreased. This is because more reductant led to smaller Co particle sizes, which could improve the BET surface area. However, the excess leads to some carbon residue in the catalyst. The surface structure of Ru promoted Co catalysts prepared by air combustion-reduction ($0.3RuCo_{\text{air-reduction}}$) and conventional ($RuCo_N$) methods from XPS spectra showed that there is a shift to lower binding energies in the energy position of the Co 2p peaks relative to the spectrum of the as-synthesized catalyst (0.3RuCo). It would seem to suggest that the cobalt oxide of the as-synthesized catalysts were presented on the surface. The reduction properties result from TPR exhibited that the presence of Ru resulted in a decrease in the reduction temperature of cobalt in RuCo catalyst. Besides, the reduction level of cobalt increased with the reductant content.

5.1.2 FTS Performances

The autocombustion RuCo catalyst exhibited the maximum activity at a moderate citric acid content (ratio of citric acid to metal was 0.3) and the initial activities of the catalysts are relative stable. For different types of reductants (at the same molar ratio of reductant to nitrate, 0.3), the catalyst prepared by citric acid

exhibited the highest activity whereas the catalyst synthesized by oxalic acid showed the lowest methane selectivity.

5.2 Iron-Based Catalysts

5.2.1 Characterization of Catalysts

The catalysts exhibited the mixed of the oxide phases and carbides phases as the detectable iron phase, indicating that the autocombustion process completed the conversion of the metal compounds to metal oxides and carbonates without further reduction.

5.2.2 FTS Performances

The CO conversion of the as-synthesized catalysts was better than that of the conventional catalysts. The catalytic activities of iron-based catalysts also depend on the contents of citric acid in the starting solution. The Fe-Cu-K with CA/N molar ratio at 0.1 exhibited highest CO conversion and relative low CH_4 selectivity compared with the other catalysts.

5.3 Conclusions

The FTS catalysts were successfully synthesized by the autocombustion method without further reduction. The results exhibited the improvement on the catalytic activity in FTS reaction. The reductant contents had a remarkable influence on controlling the structures and FTS performance of the catalysts. Furthermore, reductant types also effect on FTS catalytic activity. The FTS catalysts prepared by the autocombustion method, which omits the complex and high-energy

consumption reduction process, can be used directly for high efficiency FTS and thus will be more promising in the future.

5.4 Suggestion and Recommendation

A further study of the catalysts prepared by the autocombustion method for Fischer-Tropsch catalyst should be concerned with the following aspect:

5.4.1 The increasing in Heavy Hydrocarbon Product

Although the FTS catalysts prepared by the autocombustion method had high reduction degree compared with conventional method, it could not increase the selectivity of the heavy hydrocarbons as evidenced by low chain growth probability. The chain growth factors (alpha value) of the RuCo catalysts prepared by the autocombustion method are in the region of 0.81-0.83, which is much smaller than the conventional cobalt catalysts (about 0.88). Due to the cobalt crystalline sizes prepared by the autocombustion method were much smaller and the finely dispersed metallic crystallines were not suitable for carbon chain growth reaction. One reason for the small crystallines of our catalyst was the small pore structure. Large pore catalyst would provide the selectivity of the heavy hydrocarbons due to the high diffusion efficiency of hydrocarbon product. For further research work, large-pore silica supports with ruthenium promoter should be investigated the FTS activity.

5.4.2 The Various Types of Organic Reductants

Many organic reductant types such as formic acid, oxalic acid alanine and glycine could be used as fuel in the combustion process. Other research works

suggest that there are remarkable influences from organic reductant on the catalytic performance. The different in amount of C, H, and O atoms in organic compound can release dissimilar reducing gases during the combustion and the reducibility of the metals. Therefore, the reductant types should play an important role in controlling the structures and FTS performance of the catalysts.

5.4.3 Thermodynamics, Mechanisms and Kinetics of the FTS Catalysts Prepared by the Autocombustion Method

Studies on the thermodynamics, mechanisms and kinetics of the complexity autocombustion method are a challenging and difficult task with resulting from the great variation of factors such as reductant contents, reductant types, specific surface area and porosity of support, type of metal catalysts, type of reactor, diffusion of gaseous reagents or reaction products. The extension on the thermodynamic data calculation from the kinetic data is expected to be the useful data for further applications.

REFERENCES

1. Luque, R., et al., *Design and development of catalysts for biomass-to-liquid-Fischer–Tropsch (BTL-FT) processes for biofuels production.* Energy & Environmental Science, 2012. **5**(1): p. 5186-5202.
2. Tsubaki, N., S. Sun, and K. Fujimoto, *Different functions of the noble metals added to cobalt catalysts for Fischer–Tropsch synthesis.* Journal of Catalysis, 2001. **199**(2): p. 236-246.
3. Qian, J., et al., *High capacity Na-storage and superior cyclability of nanocomposite Sb/C anode for Na-ion batteries.* Chemical Communications, 2012. **48**(56): p. 7070-7072.
4. Schulz, H., *Short history and present trends of Fischer–Tropsch synthesis.* Applied Catalysis A: General, 1999. **186**(1): p. 3-12.
5. Sun, J., et al., *Highly-Dispersed Metallic Ru Nanoparticles Sputtered on H-Beta Zeolite for Directly Converting Syngas to Middle Isoparaffins.* ACS Catalysis, 2013. **4**(1): p. 1-8.
6. Shi, L., et al., *Surface impregnation combustion method to prepare nanostructured metallic catalysts without further reduction: As-burnt Co/SiO_2 catalysts for fischer–tropsch synthesis.* ACS Catalysis, 2011. **1**(10): p. 1225-1233.
7. Hua, Z., et al., *Sol–gel autocombustion synthesis of Co–Ni alloy powder.* Materials Chemistry and Physics, 2011. **126**(3): p. 542-545.
8. Chandradass, J., B. Jun, and D.-s. Bae, *Effect of different fuels on the alumina–zirconia nanopowder synthesized by sol–gel autocombustion method.* Journal of Non-Crystalline Solids, 2008. **354**(26): p. 3085-3087.
9. Li, F., et al., *Combustion synthesis of γ-lithium aluminate by using various fuels.* Journal of nuclear materials, 2002. **300**(1): p. 82-88.
10. Chen, W., F. Li, and J. Yu, *Combustion synthesis and characterization of nanocrystalline CeO_2-based powders via ethylene glycol–nitrate process.* Materials Letters, 2006. **60**(1): p. 57-62.

11. Marinšek, M., K. Zupan, and J. Maeek, *Ni–YSZ cermet anodes prepared by citrate/nitrate combustion synthesis.* Journal of power sources, 2002. **106**(1): p. 178-188.
12. Chakroborty, A., et al., *Preparation of low-temperature sinterable $BaCe_{0.8}Sm_{0.2}O_3$ powder by autoignition technique.* Materials letters, 2002. **57**(4): p. 862-867.
13. Hosseini Vajargah, S., H. Madaah Hosseini, and Z. Nemati, *Preparation and characterization of yttrium iron garnet (YIG) nanocrystalline powders by auto-combustion of nitrate-citrate gel.* Journal of alloys and compounds, 2007. **430**(1): p. 339-343.
14. Peng, T., et al., *Effect of acidity on the glycine–nitrate combustion synthesis of nanocrystalline alumina powder.* Materials research bulletin, 2006. **41**(9): p. 1638-1645.
15. Xu, G., et al., *Influence of pH on characteristics of $BaFe_{12}O_{19}$ powder prepared by sol–gel auto-combustion.* Journal of magnetism and magnetic materials, 2006. **301**(2): p. 383-388.
16. Yue, Z., et al., *Effect of copper on the electromagnetic properties of Mg–Zn–Cu ferrites prepared by sol–gel auto-combustion method.* Materials Science and Engineering: B, 2001. **86**(1): p. 64-69.
17. Wender, P.A., et al., *The Pinene Path to Taxanes. 4. Approaches to Taxol and Taxol Analogs through Elaboration of Aromatic C-Ring Precursors.* The Journal of organic chemistry, 1996. **61**(22): p. 7662-7663.
18. Maretto, C. and V. Piccolo, *Fischer-Tropsch process with a multistage bubble column reactor*. 1998, Google Patents.
19. Krishna, R., et al., *Gas holdup in slurry bubble columns: effect of column diameter and slurry concentrations.* AIChE Journal, 1997. **43**(2): p. 311-316.
20. Zhang, Q., J. Kang, and Y. Wang, *Development of novel catalysts for Fischer–Tropsch synthesis: tuning the product selectivity.* ChemCatChem, 2010. **2**(9): p. 1030-1058.

21. Jahangiri, H., et al., *A review of advanced catalyst development for Fischer–Tropsch synthesis of hydrocarbons from biomass derived syn-gas.* Catalysis Science & Technology, 2014.
22. Borg, Ø., *Role of Alumina Support in Cobalt Fischer-Tropsch Synthesis*. 2007, Norwegian University of Science and Technology.
23. Iglesia, E., *Design, synthesis, and use of cobalt-based Fischer-Tropsch synthesis catalysts.* Applied Catalysis A: General, 1997. **161**(1): p. 59-78.
24. Fischer, F. and H. Tropsch, *Über die direkte Synthese von Erdöl-Kohlenwasserstoffen bei gewöhnlichem Druck.(Erste Mitteilung).* Berichte der deutschen chemischen Gesellschaft (A and B Series), 1926. **59**(4): p. 830-831.
25. Lu, X., *Fischer-Tropsch Synthesis: Towards understanding*. 2012.
26. Adesina, A.A., *Hydrocarbon synthesis via Fischer-Tropsch reaction: travails and triumphs.* Applied Catalysis A: General, 1996. **138**(2): p. 345-367.
27. Arsalanfar, M., A. Mirzaei, and H. Bozorgzadeh, *Effect of calcination conditions on the structure and catalytic performance of MgO supported Fe–Co–Mn catalyst for CO hydrogenation.* Journal of Natural Gas Science and Engineering, 2012. **6**: p. 1-13.
28. MINGKUN, Z., *Mechanistic Study of Fischer-Tropsch Synthesis for Clean Fuel Production*. 2013.
29. Dictor, R.A. and A.T. Bell, *Fischer-Tropsch synthesis over reduced and unreduced iron oxide catalysts.* Journal of Catalysis, 1986. **97**(1): p. 121-136.
30. de Smit, E. and B.M. Weckhuysen, *The renaissance of iron-based Fischer–Tropsch synthesis: on the multifaceted catalyst deactivation behaviour.* Chemical Society Reviews, 2008. **37**(12): p. 2758-2781.
31. Storch, H.H., R.A. Anderson, and N. Golumbic, *The Fischer-Tropsch and related syntheses*. Vol. 6. 1951: Wiley New York.
32. Bartholomew, C.H. and R.J. Farrauto, *Fundamentals of industrial catalytic processes*. 2011: John Wiley & Sons.
33. Satterfield, C.N., *Heterogeneous catalysis in industrial practice.* 1991.
34. Steynberg, A., et al., *High temperature Fischer–Tropsch synthesis in commercial practice.* Applied Catalysis A: General, 1999. **186**(1): p. 41-54.

35. O'Brien, R.J., et al., *Activity and selectivity of precipitated iron Fischer-Tropsch catalysts.* Catalysis Today, 1997. **36**(3): p. 325-334.

36. Huang, C.-S., L. Xu, and B.H. Davis, *Fischer-Tropsch synthesis: impact of pretreatment of ultrafine iron oxide upon catalyst structure and selectivity.* Fuel science & technology international, 1993. **11**(5-6): p. 639-664.

37. Hao, Q., et al., *Activation pressure studies with an iron-based catalyst for slurry Fischer-Tropsch synthesis.* Journal of Natural Gas Chemistry, 2009. **18**(4): p. 429-435.

38. Huang, C.-S., et al., *Fischer-Tropsch Synthesis: mossbauer studies of pretreated ultrafine iron oxide catalysts.* Fuel science & technology international, 1993. **11**(9): p. 1289-1312.

39. Wang, Y. and B.H. Davis, *Fischer–Tropsch synthesis. Conversion of alcohols over iron oxide and iron carbide catalysts.* Applied Catalysis A: General, 1999. **180**(1): p. 277-285.

40. Young, R.S., *Cobalt: its chemistry, metallurgy, and uses*. Vol. 149. 1961: Reinhold Pub. Corp.

41. Zwart, R. and R. van Ree, *Bio-based Fischer-Tropsch Diesel Production Technologies.* Biofuels, 2009: p. 95-116.

42. Yu, L., et al., *Highly active Co/SiC catalysts with controllable dispersion and reducibility for Fischer–Tropsch synthesis.* Fuel, 2013. **112**: p. 483-488.

43. Ernst, B., et al., *Preparation and characterization of Fischer–Tropsch active Co/SiO_2 catalysts.* Applied Catalysis A: General, 1999. **186**(1): p. 145-168.

44. Biesinger, M.C., et al., *Resolving surface chemical states in XPS analysis of first row transition metals, oxides and hydroxides: Cr, Mn, Fe, Co and Ni.* Applied Surface Science, 2011. **257**(7): p. 2717-2730.

45. Iglesia, E., et al., *Dispersion, support, and bimetallic effects in Fischer-Tropsch synthesis on cobalt catalysts.* Studies in Surface Science and Catalysis, 1994. **81**: p. 433-442.

46. Van't Blik, H., et al., *Structure of rhodium in an ultradispersed rhodium/alumina catalyst as studied by EXAFS and other techniques.* Journal of the American Chemical Society, 1985. **107**(11): p. 3139-3147.

47. Schanke, D., et al., *Study of Pt-promoted cobalt CO hydrogenation catalysts.* Journal of Catalysis, 1995. **156**(1): p. 85-95.

48. Ho, S.-W., *Effects of Ethanol Impregnation on the Properties of Thoria-Promoted Co/SiO_2 Catalyst.* Journal of Catalysis, 1998. **175**(2): p. 139-151.

49. Iglesia, E., et al., *Bimetallic synergy in cobalt ruthenium Fischer-Tropsch synthesis catalysts.* Journal of Catalysis, 1993. **143**(2): p. 345-368.

50. Zhang, Y., et al., *A high activity Cu/ZnO/Al_2O_3 catalyst for methanol synthesis: Preparation and catalytic properties.* Applied Catalysis A: General, 1997. **158**(1): p. 105-120.

51. Bond, G., *Heterogeneous Catalysis: Principles and Applications, 1987*. Clarendon Press, Oxford.

52. Tsubaki, N., et al., *A new method of bimodal support preparation and its application in Fischer–Tropsch synthesis.* Catalysis Communications, 2001. **2**(10): p. 311-315.

53. Reuel, R.C. and C.H. Bartholomew, *The stoichiometries of H_2 and CO adsorptions on cobalt: Effects of support and preparation.* Journal of Catalysis, 1984. **85**(1): p. 63-77.

54. Rathousky, J., et al., *Hydrocarbon synthesis from carbon monoxide+hydrogen on impregnated cobalt catalysts. Part III: Cobalt (10%)/silica-alumina catalysts.* Applied catalysis, 1991. **79**(2): p. 167-180.

55. Lapidus, A., A. Krylova, and A. Zukal, *Hydrocarbon synthesis from carbon monoxide and hydrogen on impregnated cobalt catalysts II: Activity of 10% Co/Al_2O_3 and 10% Co/SiO_2 catalysts in Fischer-Tropsch synthesis.* Applied Catalysis A: General, 1992. **80**(1): p. 1-11.

56. Bechara, R., D. Balloy, and D. Vanhove, *Catalytic properties of Co/Al_2O_3 system for hydrocarbon synthesis.* Applied Catalysis A: General, 2001. **207**(1): p. 343-353.

57. Choi, J.-G., *Reduction of supported cobalt catalysts by hydrogen.* Catalysis letters, 1995. **35**(3-4): p. 291-296.

58. Wieckowski, A., E.R. Savinova, and C.G. Vayenas, *Catalysis and electrocatalysis at nanoparticle surfaces*. 2003: CRC Press.

59. Zhang, J., et al., *Recent technological developments in cobalt catalysts for Fischer-Tropsch synthesis.* Journal of Natural Gas Chemistry, 2002. **11**(3/4): p. 99-108.

60. Iglesia, E., S.L. Soled, and R.A. Fiato, *Fischer-Tropsch synthesis on cobalt and ruthenium. Metal dispersion and support effects on reaction rate and selectivity.* Journal of Catalysis, 1992. **137**(1): p. 212-224.

61. Reinikainen, M., et al., *Characterisation and activity evaluation of silica supported cobalt and ruthenium catalysts.* Applied Catalysis A: General, 1998. **174**(1): p. 61-75.

62. Panpranot, J., J.G. Goodwin Jr, and A. Sayari, *Synthesis and characteristics of MCM-41 supported CoRu catalysts.* Catalysis today, 2002. **77**(3): p. 269-284.

63. Kraum, M. and M. Baerns, *Fischer–Tropsch synthesis: the influence of various cobalt compounds applied in the preparation of supported cobalt catalysts on their performance.* Applied Catalysis A: General, 1999. **186**(1): p. 189-200.

64. Li, J., et al., *Fischer–Tropsch synthesis: effect of small amounts of boron, ruthenium and rhenium on Co/TiO_2 catalysts.* Applied Catalysis A: General, 2002. **223**(1): p. 195-203.

65. Regalbuto, J., *Catalyst preparation: science and engineering*. 2006: CRC Press.

66. Mochizuki, T., et al., *Surface structure and Fischer–Tropsch synthesis activity of highly active Co/SiO_2 catalysts prepared from the impregnating solution modified with some chelating agents.* Applied Catalysis A: General, 2007. **317**(1): p. 97-104.

67. Jiang, Y., et al., *Sol–gel autocombustion synthesis of metals and metal alloys.* Angewandte Chemie, 2009. **121**(45): p. 8681-8683.

68. Bahadur, D., S. Rajakumar, and A. Kumar, *Influence of fuel ratios on auto combustion synthesis of barium ferrite nano particles.* Journal of chemical sciences, 2006. **118**(1): p. 15-21.

69. Mali, A. and A. Ataie, *Influence of the metal nitrates to citric acid molar ratio on the combustion process and phase constitution of barium hexaferrite particles prepared by sol–gel combustion method.* Ceramics International, 2004. **30**(7): p. 1979-1983.

70. Shi, L., et al., *Surface impregnation combustion method to prepare nanostructured metallic catalysts without further reduction: As-burnt Cu–ZnO/SiO_2 catalyst for low-temperature methanol synthesis.* Catalysis Today, 2012. **185**(1): p. 54-60.

71. Wu, K., et al., *Sol–gel auto-combustion synthesis of SiO_2-doped NiZn ferrite by using various fuels.* Journal of magnetism and magnetic materials, 2006. **298**(1): p. 25-32.

72. Zhong, M.-j., et al., *Influence of citric acid content on magnetic properties of $BaFe_{12}O_{19}$ powder prepared by sol-gel auto-combustion method.* Journal of Shanghai University (English Edition), 2007. **11**: p. 263-267.

73. Abbaslou and M.R. Malek, *Iron catalyst supported on carbon nanotubes for Fischer-Tropsch synthesis: experimental and kinetic study*. 2010, University of Saskatchewan.

74. Sudsakorn, K., *Iron Fischer-Tropsch Catalysis*. 2002, University of Pittsburgh.

75. Lutz, M., *Structure/property relationships of commercial propylene/ 1-pentene random copolymers*. 2006, Stellenbosch: University of Stellenbosch.

76. PONDINI, M. and M. EBERT, *Process synthesis and design of low temperature Fischer-Tropsch crude production from biomass derived syngas.*

77. Dry, M.E., *Practical and theoretical aspects of the catalytic Fischer-Tropsch process.* Applied Catalysis A: General, 1996. **138**(2): p. 319-344.

78. Dry, M.E., *The Fischer–Tropsch process: 1950–2000.* Catalysis today, 2002. **71**(3): p. 227-241.

APPENDICES

APPENDIX A

CALCULATION FOR CATALYST PREPARATION

Reagents:

Cobalt(II) nitrate hexahydrate {$Co(NO_3)_2 \cdot 6H_2O$ (≥98%)}

Ruthenium(III) nitrate {$Ru(NO_3)_3$}

Citric acid {CA}

Silica {Q-50}

Molecular weight

Substance	Molecular weight (g/mol)
Co	58.93
$Co(NO_3)_2 \cdot 6H_2O$	291.03
Ru	101.07
$Ru(NO_3)_3$	287.09
NO_3	63.13
CA	192.12

Calculation for the preparation of RuCo catalysts *via* autocombustion method, containing 10 wt% of Co and 1 wt% of Ru over 5 g of SiO_2

Based on 100 g of catalyst used, the composition of the catalyst will be as follows:

cobalt 10 g and ruthenium 1 g

SiO_2 = 100 - (10+1) = 89 g

For 5 g of SiO_2;

Cobalt required = 5 x $\frac{10}{89}$ = 0.562 g

Cobalt 0.562 g was prepared from $Co(NO_3)_2.6H_2O$

0.562 of cobalt required from 100% $Co(NO_3)_2.6H_2O$

$$= \frac{\text{MW of Co(NO3)2.6H2O}}{\text{MW of Co}} \times cobalt\ required$$

$$= \frac{291.03}{58.93} \text{ X } 0.562$$

$$= 2.831 \text{ g}$$

So, required from 98% $Co(NO_3)_2.6H_2O$ = 2.775 g

Ruthenium required = 5 x $\frac{1}{89}$ = 0.0562 g

Ruthenium 0.0562 g was prepared from $Ru(NO_3)_3$ solution in 32 wt% dilute nitric acid (NO_3) with fraction of Ru in $Ru(NO_3)_3$ solution = 100 g /L and density = 1.262 g/ml

0.0562 g of ruthenium required $Ru(NO_3)_3$ = $\frac{1000}{100}$ x 0.0562

= 0.562 ml

Calculation of nitrate compound (N) and citric acid (CA) molar ratio (noted as CA/N)

Calculate mole of nitrate compound from $Co(NO_3)_2.6H_2O$ and $Ru(NO_3)_3$

Mole of $Co(NO_3)_2.6H_2O$ 2.775 g = $\frac{0.562}{58.93}$

= 0.0095 mol

Nitrate compound from $Co(NO_3)_2.6H_2O$ = 0.0095 x 2 = 0.019 mol

0.562 ml of $Ru(NO_3)_3$ = 0.562x1.262 = 0.709 g

Nitrate compound from 0.709 g of $Ru(NO_3)_3$ = $\frac{0.0562}{101.07}$ x 3 = 0.0017 mol

Nitrate compound from HNO_3

HNO_3 from 0.709 g of $Ru(NO_3)_3$ = 0.709 x $\frac{32}{100}$

= 0.227 g

= $\frac{0.227}{63.13}$ mol

= 0.0036 mol

Total nitrate compound = 0.019 + 0.0017 + 0.0036

= 0.024 mol

For CA/N = 0.3;

Mole of CA = 0.0072 mol

CA required = 0.0072 x 192.12 = 1.38 g

APPENDIX B

CALCULATION OF CRYSTALLINE SIZE FROM X-RAY DIFFRACTION (XRD)

The average crystalline size was calculated by:

$$D = \frac{K\lambda}{B\cos\theta}$$

D is the crystalline size (nm)

K is a constant (K = 0.89)

λ is the wavelength of X-ray (CuKα = 0.154 nm)

B is $\Delta(2\theta)$, the width of the peak at half height (radian unit)

For 0.3RuCo; 2θ at 44.134 degree, B = 1.255

2θ = 44.134 degree

θ = 22.067 degree

= $22.067 \times \frac{\pi}{180}$

= 0.385

$B = 1.255 \times \frac{\pi}{180}$

= 0.0219 radian

$$D = \frac{K\lambda}{B\cos\theta}$$

$$D = \frac{(0.89)(0.154)}{(0.0219)\cos(0.385)}$$

= 6.75 nm

APPENDIX C

EXPERIMENTAL DATA FOR FISCHER-TROPSCH SYNTHESIS

Data of experiment of 0.3RuCo catalyst for Fischer-Tropsch Synthesis

Condition of experiment : Weight of catalyst 1.006 g

: Pressure 1 MPa

: Temperature 240 °C

: Feed flow rate 14.66 ml/min

: Syngas; H_2/CO/Ar = 63.27/33.7/3.03

: Standard gas; CO/CH_4/CO_2 = 5.15/5.18/5.30

Data from Gas chromatography

Syngas (TCD)	1	2	3	Average
Ar	25602	26073	26213	25963
Co	251256	249594	250044	250298
STD gas (TCD)				
CO	40434	40619	40635	40563
CH_4	35147	35227	35251	35208
CO_2	43221	43563	43447	43410
STD (FID)				
CH_4	291011	291558	291601	291390

Data from reaction (TCD)

Time	1	2	3	4	5
Ar	41116	41272	40955	40504	41340
CO	233475	235693	235433	235581	237866
CH_4	17372	16390	15861	15303	14360
CO_2	0	0	0	0	0
F_{out}	0.0655	0.0620	0.0669	0.0679	0.0668

Data from reaction (FID, online)

Carbon	1	2	3	4	5	6	7
Orefin	0	643	18173	662	610	115	0
Parafin	200806	28432	36847	60913	56379	40238	27994
Sum	200806	29075	55020	61575	56989	40353	27994

Data from reaction (FID, offline)

Carbon	**5**	**6**	**7**	**8**	**9**	**10**	**11**
Orefin	2374	-	1101	21203	37854	26552	14812
Parafin	10131	43901	133174	589654	629645	997562	1216251
Sum	12505	43901	134275	610857	667499	1024114	1231063
Carbon	**12**	**13**	**14**	**15**	**16**	**17**	**18**
Orefin	21605	22012	16586	-	-	-	21605
Parafin	1164656	1102658	1360644	1000902	641161	703488	1164656
Sum	1186261	1124670	1377230	1000902	641161	703488	1186261
Carbon	**19**	**20**	**21**	**22**	**23**	**24**	**25**
Orefin	-	-	-	-	-	-	-
Parafin	616865	538037	464293	415849	377378	320480	287453
Sum	616865	538037	464293	415849	377378	320480	287453

APPENDIX D

CO CONVERSION AND SELECTIVIES CALCULATION

Activity of the FTS catalyst performed in term of CO conversion and reaction rate. CO conversion is defined as moles of CO convert with respect to CO in feed:

1. Calculation of percent CO conversion

0.3RuCo catalysts at the 1 hour of reaction time

$$CO\ conversion\ (\%) = \frac{\left(\frac{CO}{Ar}\right)_{in} - \left(\frac{CO}{Ar}\right)_{out}}{\left(\frac{CO}{Ar}\right)_{in}} \times 100$$

$$CO\ conversion\ (\%) = \frac{\left(\frac{250298}{29563}\right)_{in} - \left(\frac{233475}{41116}\right)_{out}}{\left(\frac{250298}{29563}\right)_{in}} \times 100$$

$$CO\ conversion\ (\%) = \frac{(9.6406)_{in} - (5.6784)_{out}}{(9.6406)_{in}} \times 100$$

$$CO\ conversion\ (\%) = 41.1\%$$

2. Calculation of selectivity of products

$$\%Selectivity = \frac{\sum_{i=0}^{n}(yield\ of\ product)_n}{(yield\ of\ all\ products)} \times 100$$

$$Yield = \frac{[(out\ flow) \times (\%CH_4)_{std} \times (FID\ area)]}{(CH_4\ area)_{std}}$$

Time at 5 hours;

$$Yield\ CH_4 = \frac{[0.0668 \times 0.0518 \times 200806]}{291390} = 2.384x10^{-3}$$

Yield of hydrocarbon;

Carbon	Yield	Carbon	Yield
1	$2.38x10^{-3}$	14	$4.57 x10^{-4}$
2	$3.38x10^{-4}$	15	$5.64 x10^{-4}$
3	$4.37x10^{-4}$	16	$4.15x10^{-4}$
4	$7.23x10^{-4}$	17	$2.66x10^{-4}$
5	$6.69x10^{-4}$	18	$2.92x10^{-4}$
6	$4.96x10^{-4}$	19	$2.56x10^{-4}$
7	$3.88x10^{-4}$	20	$2.23x10^{-4}$
8	$2.45x10^{-4}$	21	$1.93x10^{-4}$
9	$2.61x10^{-4}$	22	$1.72x10^{-4}$
10	$4.14x10^{-4}$	23	$1.57x10^{-4}$
11	$5.04x10^{-4}$	24	$1.33x10^{-4}$
12	$4.94x10^{-4}$	25	$1.19x10^{-4}$
13	$4.83x10^{-4}$	Total yield	0.0114

$$\%CH_4 \text{ Selectivity} = \frac{\sum_{i=0}^{n}(yield\ of\ CH_4)}{(yield\ of\ all\ products)} X100$$

$$\%CH_4 \text{ Selectivity} = \frac{2.38x10^{-3}}{0.0114} X100 = 20.88\%$$

VITA

Miss Rungravee Phienluphon was born on March 17, 1988 in Bangkok, Thailand. She graduated with a Bachelor's degree of Science from Department of Chemical Technology, Faculty of Science, Chulalongkorn University in 2010. She has continued her study in Ph.D. program at Department of Chemical Technology, Faculty of Science, Chulalongkorn University since 2010 and finished her study in 2014.

LIST OF PUBLICATIONS AND PRESENTATIONS

Publications:

1. Phienluphon, R., Shi, L., Sun, J., Niu, W., Lu, P., Zhu, P., Vitidsant, T., Yoneyama, Y., Chen, Q., Tsubaki, N. Ruthenium promoted cobalt catalysts prepared by an autocombustion method directly used for Fischer–Tropsch synthesis without further reduction. Catalysis Science Technology 2014, 4, 3099-3107.

2. Phienluphon, R., Pinkaew, K., Yang, G., Li, J., Wei, Q., Yoneyama, Y., Vitidsant, T., Tsubaki, N. Designing core ($Cu/ZnO/Al_2O_3$) – shell (SAPO-11) zeolite capsule catalyst with a facile physical way for dimethyl ether direct synthesis from syngas. Chemical Engineering Journal 2015.

Conference Presentations:

1. Oral presentation from the 24Th International Symposium on Chemical Engineering (ISCE-2011) in the topic of "Bio-oil production from water hyacinth by fast pyrolysis", Gyeong-ju, Korea, Dec. 2-4, 2011

2. Oral presentation from the 3rd Asian Conference on Innovative Energy & Environmental Chemical Engineering (ASCON-2012) in the topic of "Synthesis of dimethyl ether from syngas over capsule catalysts", Hualien, Taiwan, Nov. 11-14, 2012

3. Poster presentation from the 11th International Symposium on the "Scientific Bases for the Preparation of Heterogeneous Catalysts" in the topic of "Preparation of catalysts by autocombustion method for Fischer-Tropsch synthesis", Louvain-la-Neuve, Belgium, July, 6-10, 2014.